Supplemental Digital Content 2 :

Part 1. Evaluation of the genuine information integration and parameter selection of genuine permutation cross mutual information

We employed the multi-channel neural mass model (MNMM) and the surrogate data method to verify the effectiveness of the genuine permutation cross mutual information (GPCMI). The MNMM was used to assess how well the permutation cross mutual information (PCMI) performs in tracking the coupling strength. The method of surrogate data, i.e., the iterative amplitude adjusted Fourier transform (IAAFT) method, was used to generate the surrogate data to verify whether this information integration or coupling is significant or genuine [1]. The Wilcoxon signed rank test was used to detect the GPCMI. A p-value of 0.001 was set as the threshold for significance testing. Selection of PCMI parameters was also discussed.

1.1 Multi-channel neural mass model

In the study of [2], a modified MNMM was proposed and employed to evaluate whether the synchronization measures can track the changes in coupling strength in multivariate neural data. The neural mass model (NMM) has been proven to be effective in simulating real neural oscillations[3-6], especially for intracranial electroencephalogram (EEG) recordings [7,8]. In this study, we applied the MNMM to generate two coupled neural populations to test the performance of the PCMI, and used the surrogate method to verify the effectiveness of genuine PCMI measurements. The schematic diagram of the MNMM is shown in Figure S1. Because we only considered the coupling between two channels, only two areas are illustrated in the figure.

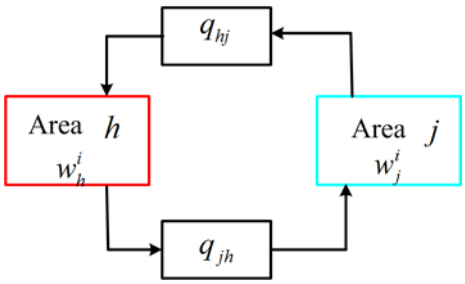

Figure S1. Schematic diagram of a two-channel neural mass model.

The areas h and j represent two EEG channels. The coupling coefficient q_{jh} indicates the coupling between area h and area j. The weighting parameters w_j^i and $i = 1,2,\ldots,N$ were used to adjust the multi-kinetics in the MNMM.

Detailed information on the MNMM has been covered in the study of [2] and here is a brief description of how it works.

In each area, we used a multi-kinetics neural mass model to generate a channel of neural activities [9]. There are N parallel subpopulations in each area and each subpopulation has its kinetics. The weight parameters w_j^i and $i = 1,2,\ldots,N$ were used to determine the relative size of each subpopulation. The parameter w_j^i needs to satisfy two conditions: $w_j^i \in [0,1]$ and $\sum_{i=1}^{N} w_j^i = 1$. q_{jh} and q_{hj} denote the coupling coefficient between areas j and k.

The following set of differential equations governs the MNMM:

$$\begin{cases} \dot{y}_0^{ji} = y_3^{ji} \\ \dot{y}_1^{ji} = y_4^{ji} \\ \dot{y}_2^{ji} = y_5^{ji} \\ \dot{y}_3^{ji} = \dfrac{H_e^i}{\tau_e^i} \cdot S\left(\sum_{i=1}^{N} w_j^i y_1^{ji} - \sum_{i=1}^{N} w_j^i y_2^{ji} \right) - \dfrac{2y_3^{ji}}{\tau_e^i} - \dfrac{y_0^{ji}}{(\tau_e^i)^2} \\ \dot{y}_4^{ji} = \dfrac{H_e^i}{\tau_e^i} \cdot \left[p_j(t) + C_2 S\left(C_1 \sum_{i=1}^{N} w_j^i y_0^{ji} \right) \right. \\ \qquad \left. + RM\left(\sum_{k=1,k\neq j}^{M} q_{jk} S\left(\sum_{i=1}^{N} w_k^i y_{1\_\tau}^{ji} - \sum_{i=1}^{N} w_k^i y_{2\_\tau}^{ji} \right) \right) \right] \\ \qquad - \dfrac{2y_4^{ji}}{\tau_e^i} - \dfrac{y_1^{ji}}{(\tau_e^i)^2} \\ \dot{y}_5^{ji} = \dfrac{H_i^i}{\tau_i^i} \cdot C_4 S\left(C_2 \sum_{i=1}^{N} w_j^i y_0^{ji} \right) - \dfrac{2y_5^{ji}}{\tau_i^i} - \dfrac{y_2^{ji}}{(\tau_i^i)^2} \end{cases} \tag{1}$$

The simulated EEG signal of channel j is represented as:

$$EEG_j = \sum_{i=1}^{N} w_k^i y_{1\_\tau}^{ji} - \sum_{i=1}^{N} w_k^i y_{2\_\tau}^{ji}$$

Where $j = 1,2,\ldots,M$ represents the channel number; $i = 1,2,\ldots,N$ represents N parallel subpopulations; H_e and H_i are the average grain of excitatory and inhibitory synapses, respectively; τ_e and τ_i represent the sum of the rate constants of passive membrane as well as other spatial delays in dendritic tree of excitatory and inhibitory inputs, respectively. The parameters C_1, C_2, C_3 and C_4 represent the average numbers of synaptic connections between the inter-neurons and pyramidal cells. The function $S(v) = 2e_0 / (1 + e^{r(v_0 - v)})$ was used to transform the average membrane potential of neural population into an averaged action potential which was fired by the neuronal networks. $p_j(t)$ represents a Gaussian noise from other

uncertain areas and as the input of area j. The module $C_2S(C_1\sum_{i=1}^{N} w_j^i y_0^{ji})$ represents the excitatory feedback from pyramidal cells. The module $RM(\sum_{k=1,k\neq j}^{M} q_{jk} S(\sum_{i=1}^{N} w_k^i y_{1\_\tau}^{ji} - \sum_{i=1}^{N} w_k^i y_{2\_\tau}^{ji}))$ represents the coupled signal from other areas. $y_{1\_\tau}^{ji}$ and $y_{2\_\tau}^{ji}$ represent the coupled signals with a propagation time (τ). In order to ensure a equilibrium between each population, the mean value was removed from the coupling signals based on the function $RM(x) = x - mean(x)$.

In this study, we only simulated two EEG time series ($M = 2$). Some important parameters were set as follow: (1) The number of subpopulations was set as $N = 3$. (2) The extrinsic inputs $p_j(t)$ were set to the same mean value $\langle p_j \rangle = 220$ and standard deviation $\sigma_{p_j} = 22$. (3) The sampling rate was set to 500 Hz. (4) The lag of propagation was set as $\tau = 10$ ms. (5) The weight parameters were set as $W = [w_j^1, w_j^2, w_j^3] = [0.635, 0.3, 0.065]$. (6) The coupling strength was set to a value ranging from 10 to 25. Values set for other parameters in the MNMM can be found in [9].

1.2 EEG recordings of two channels during propofol anesthesia

Whether the factors of volume induction and epileptic foci have any impact on the PCMI indices cannot be verified in this study. So to achieve optimal parameters for the embedding dimension and lag in the PCMI, we employed a new set of EEG data, which was recorded from volunteers during propofol anesthesia [10,11] . The experimental paradigm details and the subjects' information can be found in the study of [10,11], and here is a quick explanation. Nine human volunteers (6 males and 3 females aged from 18-42) were recruited to undergo a brief propofol administration. The propofol was infused intravenously at a speed of 150 ml/h by using a syringe driver pump. The EEG data from the positions Fp1-F7 and C3-T3 were recorded by the BIS monitor (Aspect Medical System, Natick, MA, USA). The sampling rate of raw EEG signals is 256 Hz, and the BIS value is sampled at a the frequency of 0.2 Hz. The EEG recordings of these two channels are displayed in bipolar montages, which eliminates the common source problem [12].

The EEG preprocessing procedures in this study were the same as those used in our previous study. The electrooculogram (EOG) and electromyogram (EMG) were attenuated by using a stationary wavelet transform and an inverse filter [13]. The main noise was cancelled by an adaptive noise canceling method [14]. After these procedures were complete, the EEG signals were resampled to 100 Hz for analysis.

1.3 Criteria for selection of permutation cross mutual information parameters

Before getting started on the calculation, we analyzed the selection of PCMI parameters. The PCMI is derived by using the theories of mutual information and permutation entropy. There were

three parameters to be considered: the embedding dimension m, the time lag τ, and the epoch length L.

(1) Bant et al. suggested that m ranged in 3-7 is a reasonable setting in calculation [15]. If the embedding dimension is smaller than 3, the algorithm would not work well due to the small number of patterns. Whereas, when $m > 7$, more computing time and longer data series are required. In our previous studies [8,14], we found the embedding dimension m is suitable for EEG analysis when it is within the range of 3 to 6. The PCMI can only capture 6 ($3!$) symbolic patterns when $m = 3$, which is relatively small for complex EEG oscillations. When $m \geq 5$, the epoch length (L) must be more than 14400 ($5!5!$) points [14] in order for every possible joint symbolic pattern to happen in the calculated epoch. It means that a data length of more than 144 s is needed to guarantee a reasonable PCMI value under the sampling rate of 100 Hz. With this data length, the real-time changes in time-varying dynamics cannot be well captured, and the computing time will increase rapidly. Therefore, we selected $m = 4$ in this study, which only requires 576 points (5.76 s) for calculation and has been proven to be suitable for EEG analysis during anesthesia in our previous study [14].

(2) The parameter lag τ is the number of sample points spanned by each section of the motif. It supplies the resultant fraction features of the motifs [8]. The selection of the lag is associated with the sampling rate and signal characteristics. Higher sampling rates and lower frequency oscillations require a longer lag. Three criteria were used to select the lag [16]. The first one is based on the autocorrelation function (ACF) [8]. When the value of a normalized ACF is less than e^{-1}, the corresponding lag τ is optimal. The second criterion is based on the mutual information, i.e., the lag τ corresponding to the maximal mutual information value is an optimal choice. The third criterion, which is the most important one, is the ability to discriminate different dynamic states in real application. The optimal parameter should be robust enough to track the changes in the coupling strength. To facilitate real application in depth of anesthesia (DoA) monitoring, it is important to consider the ability to discriminate different conscious states (i.e., the wakeful and unconscious states) [11,17]. A detailed description of how to select lag τ for the model and EEG data is provided in section 1.5.

(3) When selecting the parameter for epoch length, the following factors must be considered. Firstly, the epoch length L needs to meet the condition of $L > m!m!$. In this study, we selected the $m = 4$ as the optimal parameter for model and electrocorticogram (ECoG) data analysis, with the shortest L being 576 points (i.e., 5.76 s under the sampling rate of 100 Hz). Secondly, to guarantee every possible motif pattern occurs more than once in calculating the joint probability, the number of the motifs in one epoch should meet the condition of $L - \tau(m-1) > m!m!$, which requires the epoch length to meet the condition of $L > m!m! + \tau(m-1)$. Thirdly, as covered in a previous comment, the ability to discriminate different states is also an important criterion for parameter selection. In this study, we selected a data length of 10 s and an overlap rate of 75%, which are sufficient to capture the changes in time-varying dynamics and meet the requirements for PCMI calculation.

1.4 Statistics and evaluation criteria

To verify the performance of the PCMI in tracking the coupling strength of the model, we employed the degree of monotonicity (DoM) as a referee [18]. The formula of the DoM is as follows:

$$DoM = \frac{2}{r(r-1)} \sum_{i=1}^{r-1} \sum_{j=i+1}^{r} sign(s_j - s_i) \tag{2}$$

Where s_i and s_j are the coupling measure indices (i.e., PCMI) at monotonously-increased coupling strengths. The range of i and j is $i, j = 1, 2 \ldots, r$, where r is the number of the discretized coupling strengths. If the indices of s increase monotonically as the coupling strength ε enhances, then $s_i < s_j, i \leq j$. If the increase in the sequence $s_1, s_2, \cdots, s_r$ is strictly monotonous to the coupling strength, $DoM = 1$, it indicates that the measurement is linearly correlated with the coupling strength. Whereas, $DoM = 0$ means that the measurement cannot predict the increase in the coupling strength. $DoM = -1$ means the indices decrease monotonically as the coupling strength increases.

Box plots were used to evaluate how well the PCMI performs in distinguishing the wakeful and unconscious states. The prediction probability (P_k) and Pearson correlation coefficient (R) were used for evaluating the performance of the PCMI in tracking the BIS and effect-site concentration (C_{eff})[11].

1.5 Results

(1) Selection of parameter τ for model and real ECoG data.

Figure S2 shows the changes in normalized ACF values with the lag τ in the range from 0 to 20 in model (Figure S2A) and ECoG data (Figure S2B). It can be seen that the lag τ should be greater than 18 and 15, respectively, to be suitable for the MNMM and ECoG data. However, the distribution of the maximum mutual information shows there is no unique optimal lag in MNMM and ECoG signals. For example, in Figure S3 (A), suitable options for the MNMM include 1, 19, and 20. Based on the selection criteria of ACFs, we selected lag $\tau = 19$ for calculating the PCMI of the MNMM. Selection of the optimal parameter for real data based on the mutual information was completely different from that based on ACFs. The mutual information shows that 1 is the optimal option for lag. Studies in real application suggested that lag $\tau = 1$ is suitable for EEG analysis during anesthesia [14,19]. Figure S4 shows a segment of 1 s of ECoG data, the solid black line and dash black represent $\tau = 1$ and 15, respectively. Under the sampling rate of 100 Hz, lag $\tau = 1$ means that the time span of the motif is 10 ms, whereas, $\tau = 15$ indicates that the symbolic pattern can only capture time spans longer than 150 ms. In another word, when lag $\tau = 15$, the PCMI cannot characterize the dynamic changes in frequencies higher than 6.67

Hz, such as alpha (8-15 Hz), beta (16-31 Hz) and gamma (> 32 Hz) oscillations. Therefore, the ACF is not a suitable criterion for selecting parameters for real ECoG data.

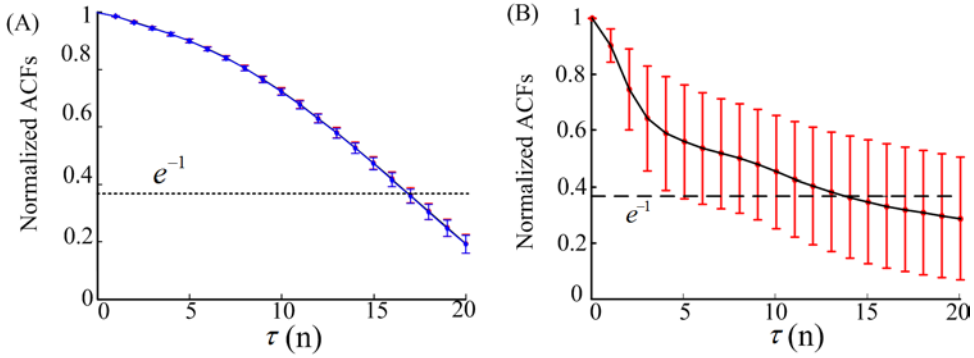

Figure S2. The mean ± SD of normalized ACF under different lag τ values in MNMM (A) and ECoG data (B).

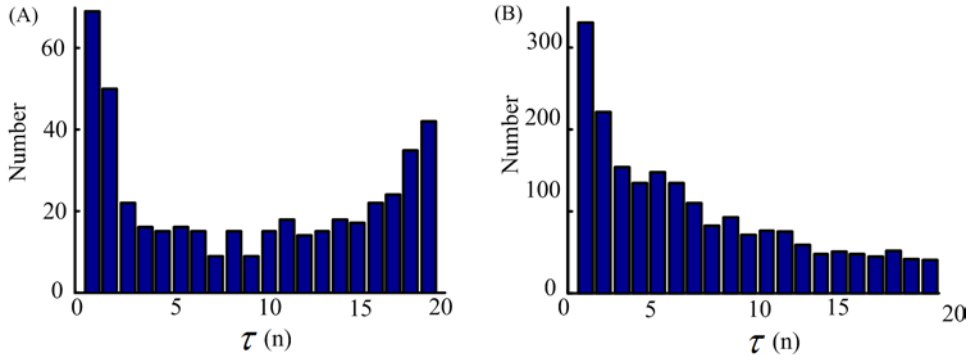

Figure S3. Distribution of the maximal mutual information values under different lag τ values in MNMM (A) and ECoG data (B).

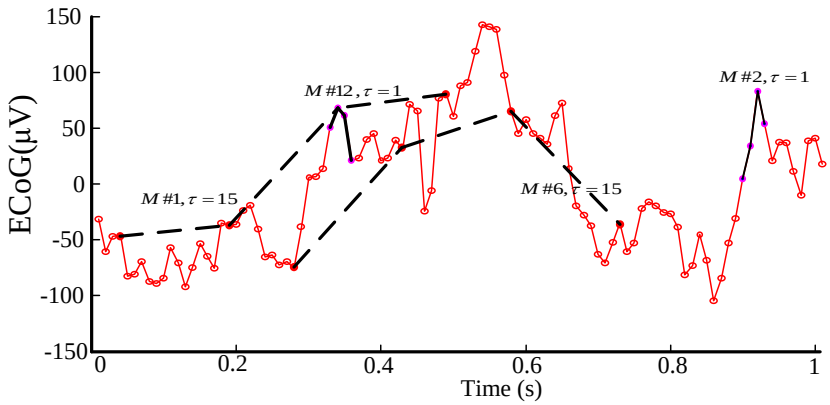

Figure S4. Diagram of ECoG signals when lag $\tau = 1$ and 15.

In the study of [20], the authors proposed a weight symbolic mutual information (wSMI) method, which works in a similar way to the PCMI, to analyze the differences among the consciousness states (vegetative state (VS), minimally conscious state (MCS), and conscious state (CS)). Due to the short trials duration (~ 800 ms) and the high sampling rate (250 Hz), they only considered the condition when $m = 3$ and lag $\tau = 8$, 16, and 32 ms. It was found that the wSMI method performs better in discriminating the VS, MCS, and CS when $\tau = 16$ and 32 ms.

Taking into account these empirical choices, we further analyzed the performance of the PCMI when $\tau = 1$, 2, and 3 (10, 20, and 30 ms under the sampling rate of 100 Hz). The ECoG

signals we analyzed were recorded from the epilepsy patients, which involved abnormal discharges that may lead to unjustified measurement [21]. Therefore, another data set recorded from healthy participants was employed for parameter selection. Two channels of preprocessed EEG signals from one subject and corresponding PCMI measurements are shown in Figure S5. It can be seen that the PCMI indices curve when $m = 4$ and $\tau = 1$ (PCMI41) moves in the opposite direction to C_{eff}. Whereas, the PCMI indices show an increasing trend in unconscious state (during the interval between the loss of consciousness (LOC) and recovery of consciousness (ROC) time points) when $\tau = 2$ and 3 (PCMI42 and PCMI43). Evaluation of the prediction probability P_k and correlation coefficient R revealed that the PCMI41 has higher P_k and R values with BIS and C_{eff} than the PCMI42 and PCMI43 (see Figure S6). The mean ± stand deviation (SD) values of all measurements are shown in Table S1. Furthermore, the box plots presented in Figure S7 indicate that the PCMI41 can clearly distinguish the awake (I), deep anesthesia (III), and RoC (IV) states ($p<0.001$, Kruskal-Wallis H test and Multiple comparison test). However, the PCMI43 can distinguish none of these three states ($p>0.05$, Kruskal-Wallis H test and Multiple comparison test), and the PCMI42 fails to distinguish the awake and RoC states ($p>0.05$). All these results indicate that the PCMI performs the best in analyzing the EEG data during anesthesia when the embedding dimension is $m = 4$ and $\tau = 1$. Therefore, we selected $m = 4$ and $\tau = 1$ as the optimal parameters for ECoG analysis. The ECoG signals were also resampled to 100 Hz.

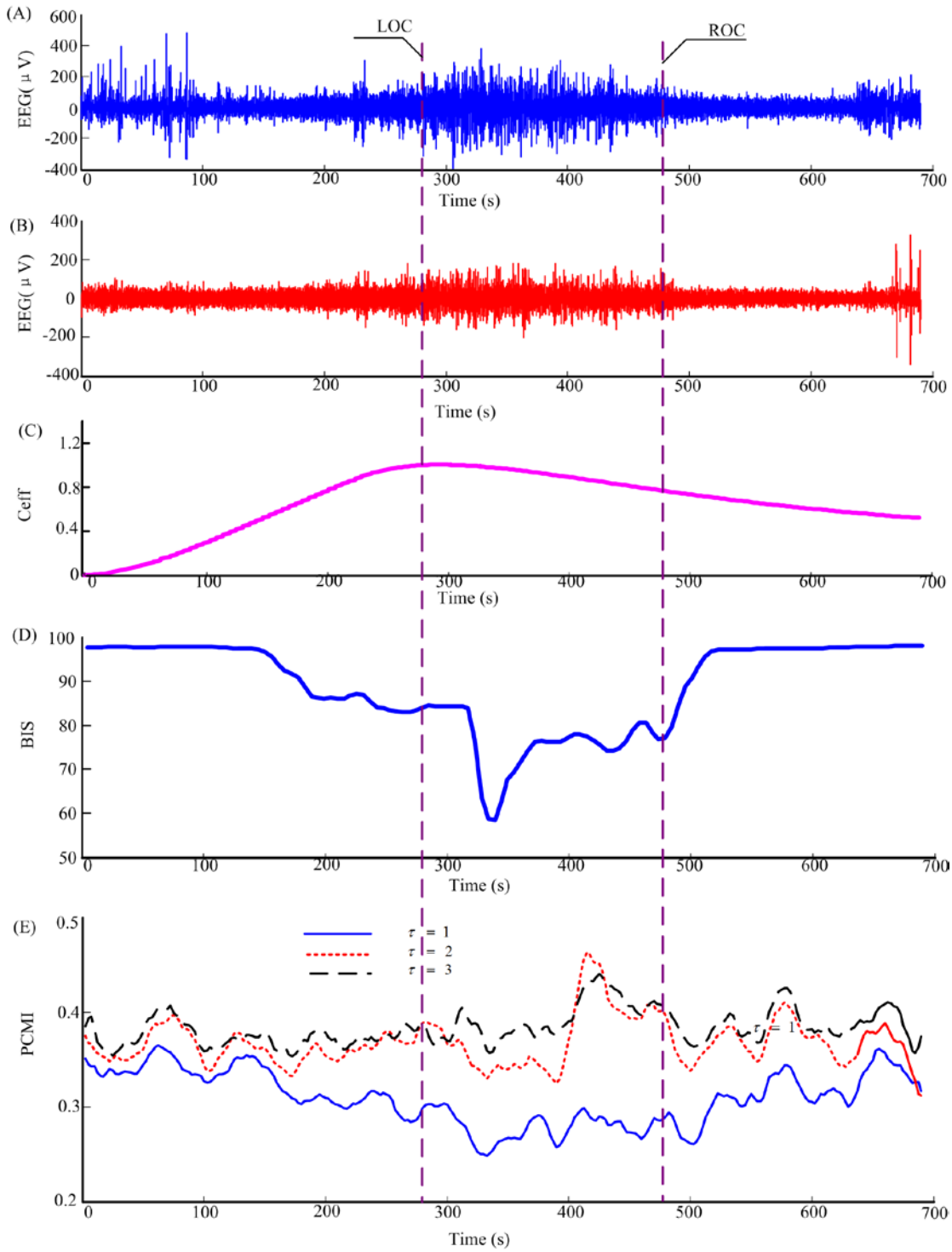

Figure S5. Two channels of preprocessed EEG signals of one subject and corresponding indices over the whole experiment. (A) and (B): the EEG recordings from the positions of Fp1-F7 and C3-T3, respectively. (C): The C_{eff} values of one subject. (D): the BIS value of one subject. (E): The PCMI measurements when $m = 4$, lag $\tau = 1$, 2, and 3.

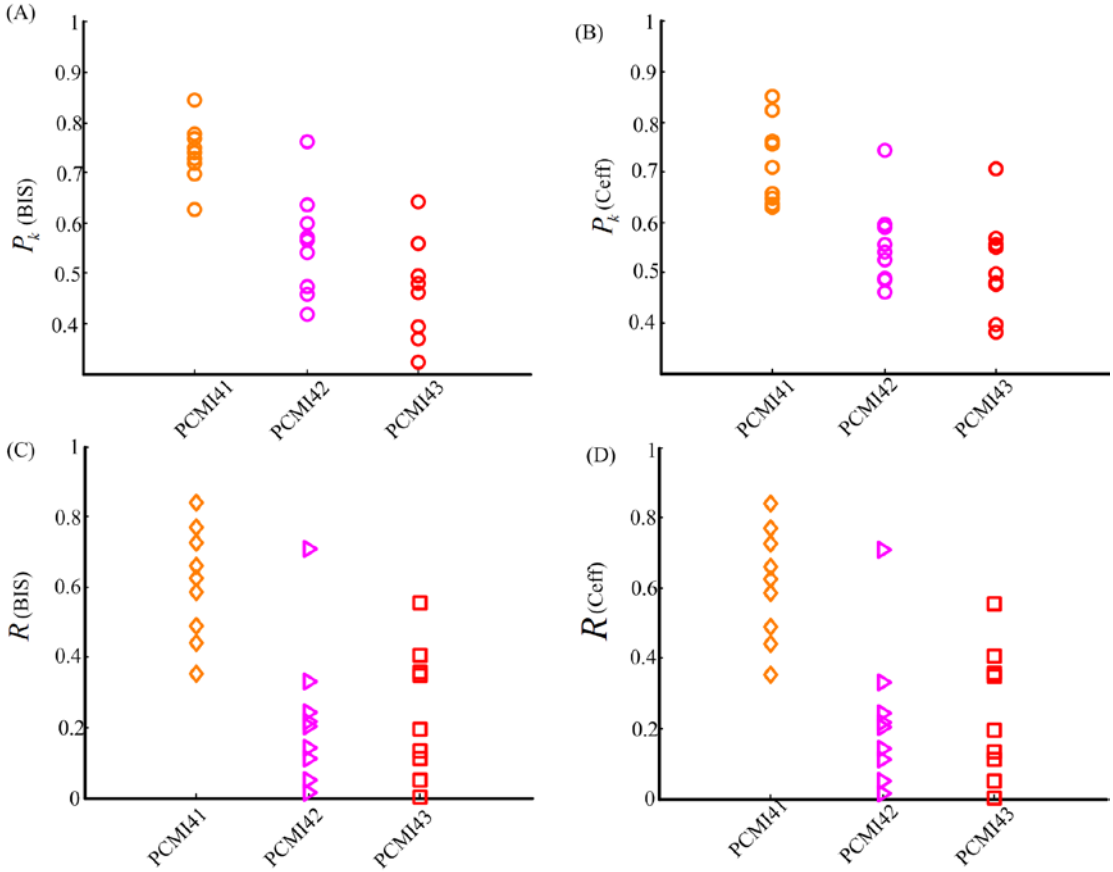

Figure S6. The prediction probability P_k and correlation coefficient R values of PCMI indices. (A): The P_k of PCMI indices with BIS of all subjects with the lag $\tau = 1$, 2, and 3 (PCMI41, PCMI 42, and PCMI 43, respectively). (B): The P_k of PCMI indices with C_{eff} of all subjects with the same parameters as in (A). (C) and (D): The R values of PCMI indices of all patients with BIS and C_{eff}, respectively.

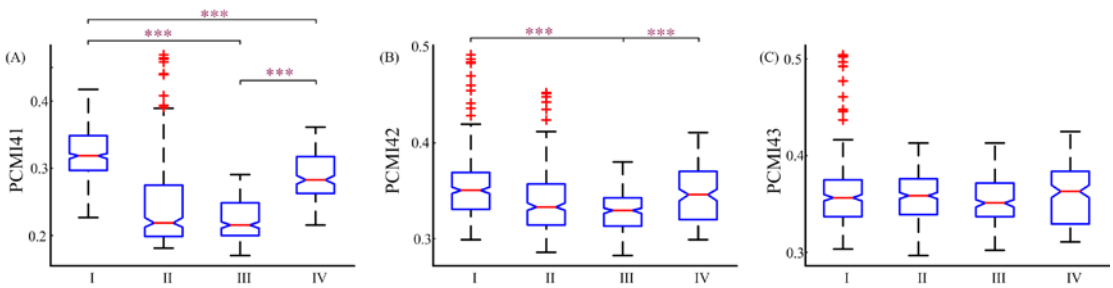

Figure S7. Box plots of the PCMI when lag $\tau = 1$, 2, and 3 (PCMI41,PCMI42, and PCMI43) in the awake (I), induction (II), deep anesthesia (III), and recovery of consciousness (IV) states.

Table S1: PCMI statistics in different states.

	Awake	Induction	Deep anesthesia	RoC

	median(Q1,Q3)	median(Q1,Q3)	median(Q1,Q3)	median(Q1,Q3)
PCMI41	0.32(0.29,0.35)	0.22(0.20,0.27)	0.22(0.20,0.25)	0.28(0.26,0.32)
PCMI42	0.35(0.33,0.37)	0.33(0.31,0.36)	0.33(0.31,0.34)	0.35(0.32,0.37)
PCMI43	0.36(0.34,0.37)	0.35(0.34,0.38)	0.35(0.34,0.37)	0.36(0.33,0.38)

(2) The performance of genuine permutation cross mutual information in assessing the coupling model

The performance needs to be verified from two perspectives. One is how well the PCMI performs in tracking the coupling strength, which was verified the MNMM. The other one is the genuine or significant connection between the two channels in ECoG as detected by the GPCMI, the performance of which was verified by the MNMM and surrogate data analysis.

Cui et al. suggested that the simulated EEG time series exhibit a weak coupling when the coupling coefficient ranges from 10 to 14 and a strong one when the coefficient is greater than 23 [2]. In this study, we analyzed the PCMI changes with a coupling strength from 10 to 25. Figure S8 shows the simulated EEG time series and the corresponding measurements (PCMI, phase locking value (PLV), and coherence (COH)). As shown in Figure S8B, the PCMI value increases linearly with the coupling strength. The surrogate PCMI indices in every coupling strength (step=0.2) are also represented in box plots. It can be seen that the PCMI value is higher than the three-quarters of the median of surrogate PCMI when the coupling coefficient is greater than 12.2. The significance analysis indicated that the distribution of the PCMI values deviates significantly from that of the surrogate PCMI values ($p<0.001$, Wilcoxon signed rank test) when the CC is greater than 12.

Based on the analysis of the MNMM, we concluded that combined use of the PCMI and the surrogate method (IAAFT) has the power to assess the coupling of nonlinear systems.

Furthermore, we compared the performance of the PCMI with that of PLV and COH based on the DoM in the MNMM. The results show that the PCMI has higher DoM values than PLV and COH (0.87, 0.83, and 0.75, respectively). This indicates that the PCMI does a better job than PLV and COH at tracking the coupling of nonlinear systems.

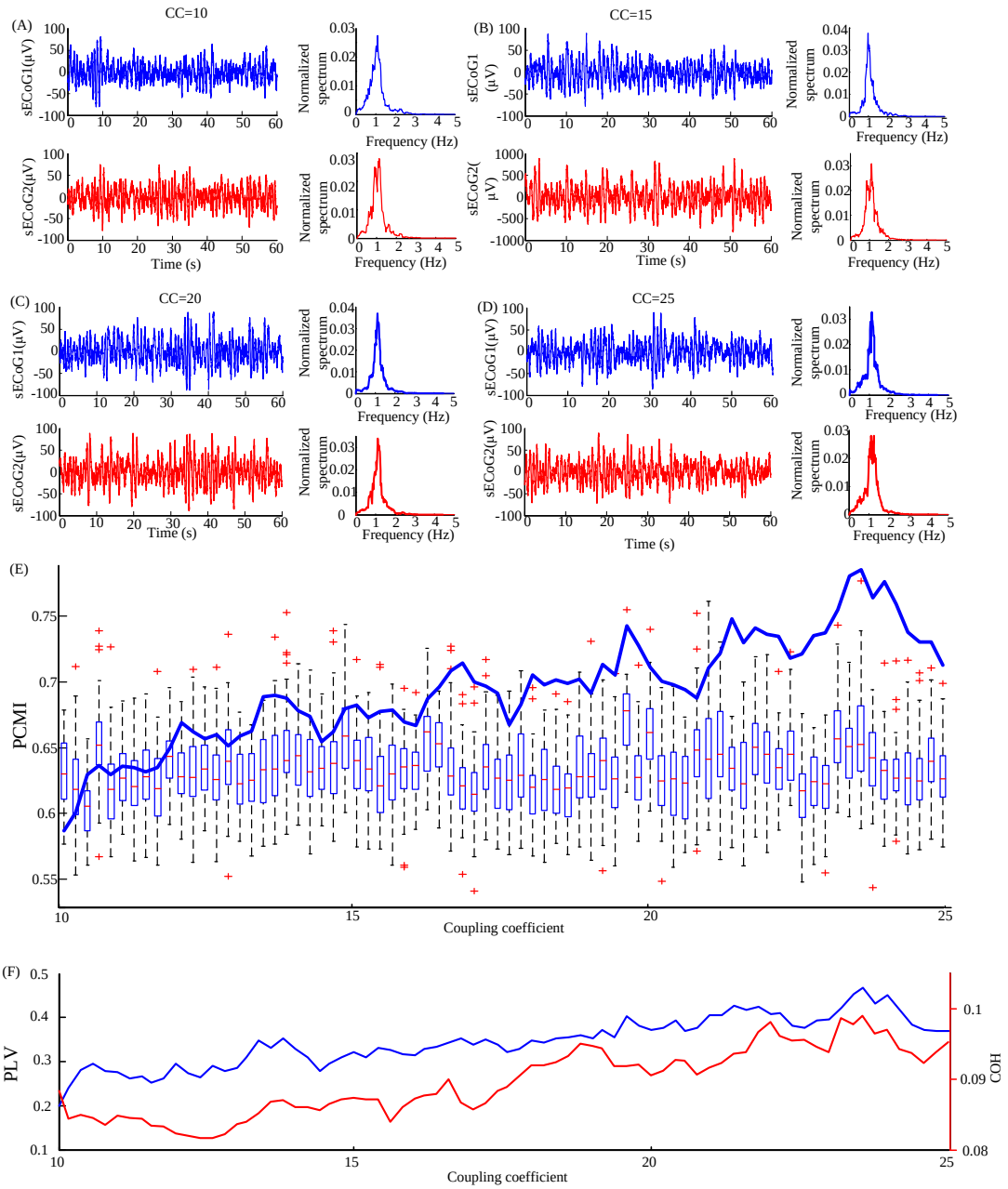

Figure S8. PCMI analysis of the MNMM model. (A)-(D): The time series of two simulated neural oscillations when the coupling coefficient $CC = 10$, 15, 20, and 25 (left part in each sub-figure) as well as their corresponding normalized power spectrum (right part in each sub-figure). (E): The PCMI curve and the box plots of the surrogate PCMI indices in each coupling strength (step=0.2). (F): The changes in PLV (blue curve) and the coherence (red curve) with the increase of CC.

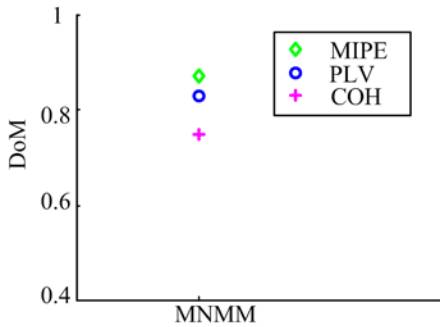

Figure S9. The DoM values of PCMI, PLV, and COH for the MNMM.

Part 2. Evaluation of the influence of spiking on permutation cross mutual information measurement

For abnormal spiking, existing studies found that interictal spike activities exist in ECoG among patients with refractory epilepsy during sevoflurane, isoflurane, and dexmedtomidine anesthesia [22-24]. The interictal spike frequency increases as the minimum alveolar anesthetic concentration (MAC) increases. Recently, there are two contradictory view points on abnormal spiking for the propofol anesthesia. Some studies suggested that propofol suppresses spontaneous epileptiform EcoG, while some reported that spike activities increase during propofol anesthesia and propofol might lower the seizure threshold of the brain and induce epileptiform spikes [24,25]. Some studies have discussed the features of epileptiform spikes, such as large amplitude spikes during seizure (>100 μV) and significant negative polarity [23,24]. The induction anesthetic used in this study is propofol. The ECoG signals in both wakeful and unconscious states are shown in Figure S10. Spike activities can be seen both in wakeful and unconscious states in this patient. Channels 1, 2, and 9 are near the epileptogenic foci. In unconscious state, there are a higher number of spike activities in Channels 1 and 2 than in Channels 8 and 9. There are about 5 spikes in Channel 1 in the epoch length of 10 s. Methods such as continuous wavelet transform [26] and template-based detection [27] have been proposed to detect spiking in EEG analysis. Because abnormal spike activities come with complex and diverse morphological characteristics, it is still hard to eliminate all the spike activities from ECoG recordings. Considering that this study is not intended to eliminate epileptiform spikes, we directly verified whether the PCMI is sensitive to abnormal spiking. Our previous study demonstrated that permutation entropy is not sensitive to spiking [28].

A simulation method was finally chosen. The multi-channel neural mass model (MNMM) was used to generate two coupled neural oscillations. Then, several epileptiform spike templates were extracted from the real ECoG recordings. The study of [22] has shown that the number of spikes in an epoch length of 10 s is less than 10 during 0.3 MAC and 1.5 MAC isoflurane anesthesia. Whereas, the number of spikes during 1.5 MAC sevoflurane anesthesia is greater than 10 in most patients. Further, the maximum spiking rate during dexmedtomidine anesthesia is 12 spikes/3 min [24] Based on the information provided by epileptologists (TY) from Xuanwu Hospital, Beijing, China, we found that no more than 10 spikes occur within a recording length of 10 s (see Figure S10). Therefore, we generated two coupled MNMM signals, which added the spike templates at a random position, with the number of spikes being 2 to 10. Figures S11 (A) and (B)

show two coupled MNMM signals and simulated signals which added 4 spikes. The PCMI was used to measure the changes in coupling strength as the coupling coefficient changes from 10 to 25 with a step of 0.2. Figure S11 (E) shows the PCMI values of the coupled model with different numbers of spikes. It can be seen that the PCMI value decreases as the number of spikes increases. However, the PCMI curves reflect an increase in coupling even when the number of spikes is 10. When the number of spikes is 10, the PCMI values show a 0.02 ± 0.01 deviation (mean ± standard deviation) to those of the original model data. Spiking only causes a 2%~3% offset from the original PCMI, indicating that it has a slight impact on PCMI-based coupling measurement.

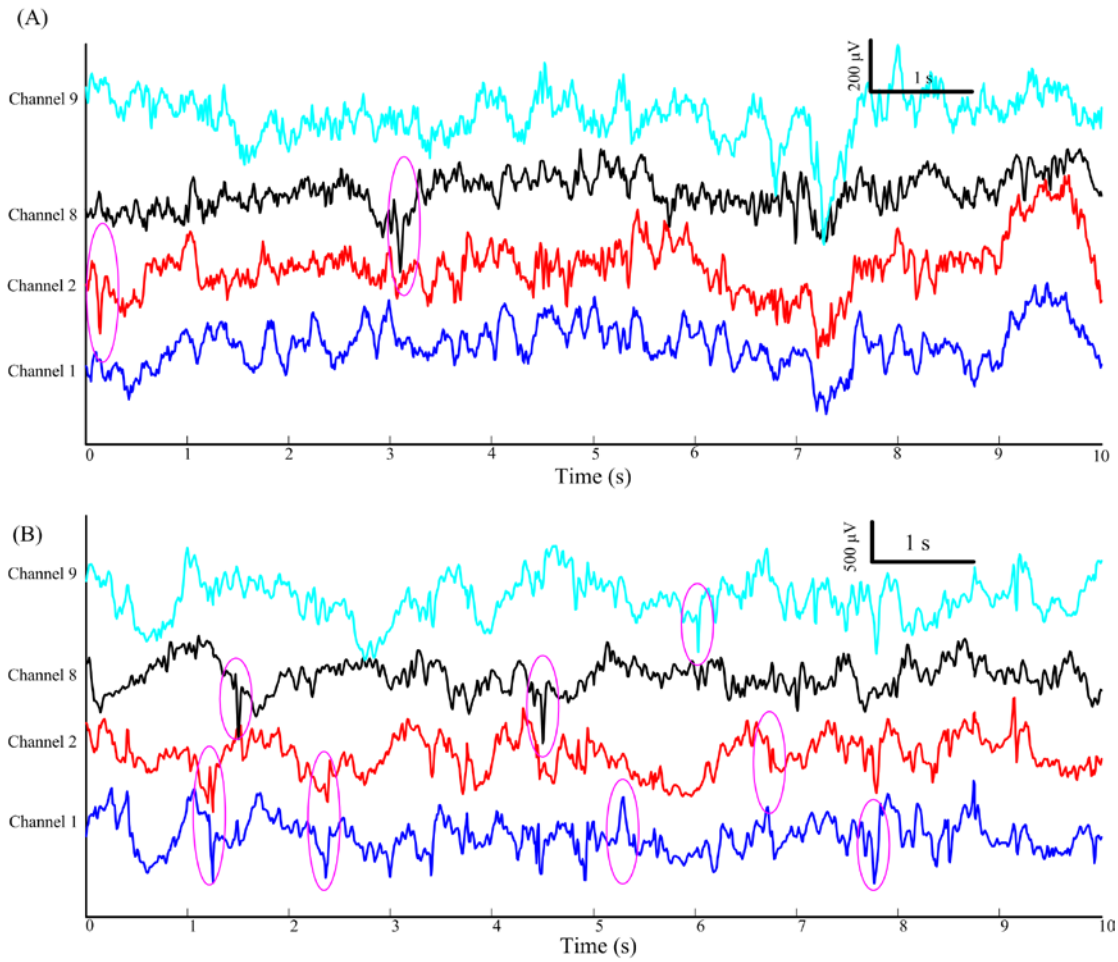

Figure S10. Four channels of ECoG signals in awake (A) and unconscious (B) states.

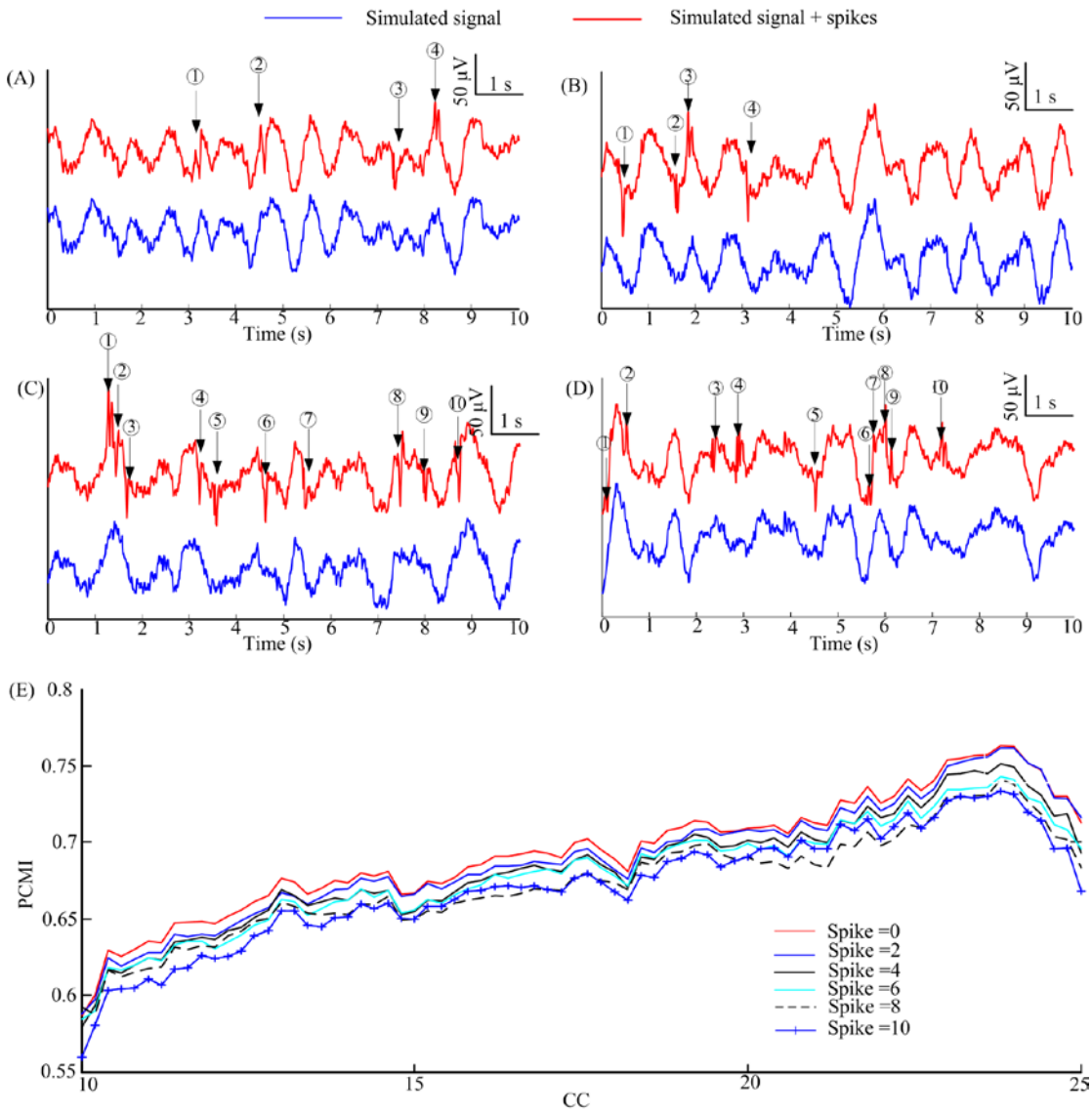

Figure S11. (A) and (B): Two coupled MNMM signals with 4 spikes (in red) and no spike (in blue). (C) and (D): Two coupled MNMM signals with 10 spikes (in red) and no spike (in blue). The PCMI values of two coupled MNMM signals with a couple coefficient (CC) from 10 to 25.

Part 3. Analysis and elimination of volume conduction effects

In the context of EEG/MEG, the term "volume conduction effects" is refers to the recording of an instantaneous linear mixture of the multiple brain source activities by each EEG/MEG channel [29]. Volume conduction effects are an important issue in EEG/MEG data analysis. The brain source activities are spread out across a sensor space (EEG/MEG channels) when they pass through the space from the cortical to the scalp. Although the ECoG signals are recorded from the surface of the cortical, volume conduction effects still cannot be neglected given the close proximity between the recording electrodes. Signals from short-distance electrodes might appear very similar. Therefore, efforts to obtain such spatial resolution could be unjustified [21]. Also, volume conduction effects may lead to the measurement of spurious functional couplings among EEG channels that are not caused by brain interactions [29].

In this study, we found that some PCMI values increase after LOC when the electrode distance is less than 3 cm, and this is especially the case when the distance is less than 1 cm (see Figure 4). This is an interesting phenomenon. However, many studies suggested that signals derived from short-distance electrodes might appear very similar, which may lead to unjustified spatial resolution measurement [21,29,30].

We reanalyzed the same ECoG signals, as shown in Figure 4. The lag values and correlation coefficients among two of these four electrodes in wakeful and unconscious states are shown in Figures S12 and S13. We used the cross-correlation function (*xcorr.m*) to measure the cross correlation under different lag (time point) values [31]. The lag corresponding to the maximal correlation value was determined as the lag between two signals. In this study, we only considered correlation coefficient values greater than 0.5 (highly correlated). The lag values with short-distance electrodes (1-2, 1-9, and 2-9) are close to zero (less than 10 ms). It means that the ECoG signals are highly correlated particularly over short distances. Whereas, the time points corresponding to the peak correlation value in the long-distance electrodes (1-8, 2-8, and 8-9) are far from zero (more than 20 ms), especially in unconscious state. The correlation values of Channels 8-9 both in awake and unconscious states are less than 0.3. This indicates that there exists no obvious correlation between these two channels over long distances. We hypothesized that short-distance electrodes with near zero phase-difference (lag=0) and high correlation values might be subject to volume conduction effects due to the common source problem [32].

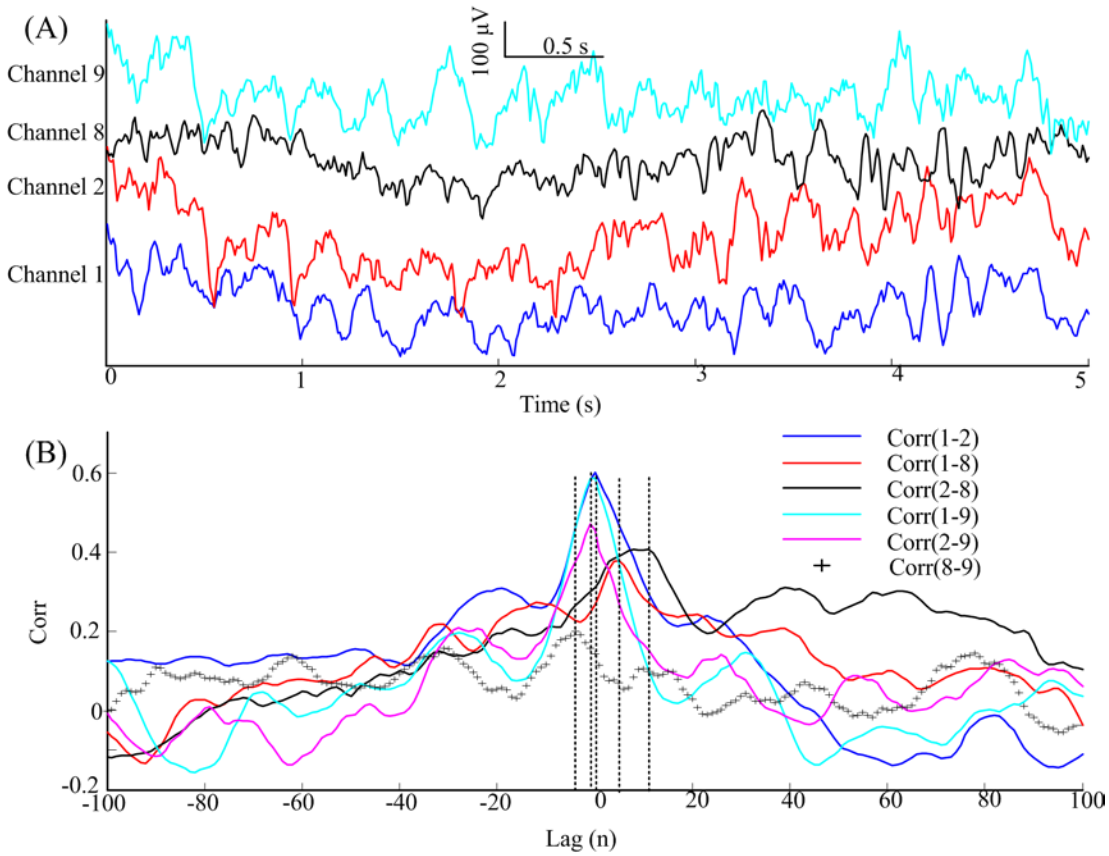

Figure S12. The lag and correlation coefficients of four channels from one subject as shown in Figure 4 in the awake state. (A): The ECoG waveforms with Channels 1, 2, 8, and 9. (B): The cross correlation between two ECoG signals under different lag values as shown in (A).

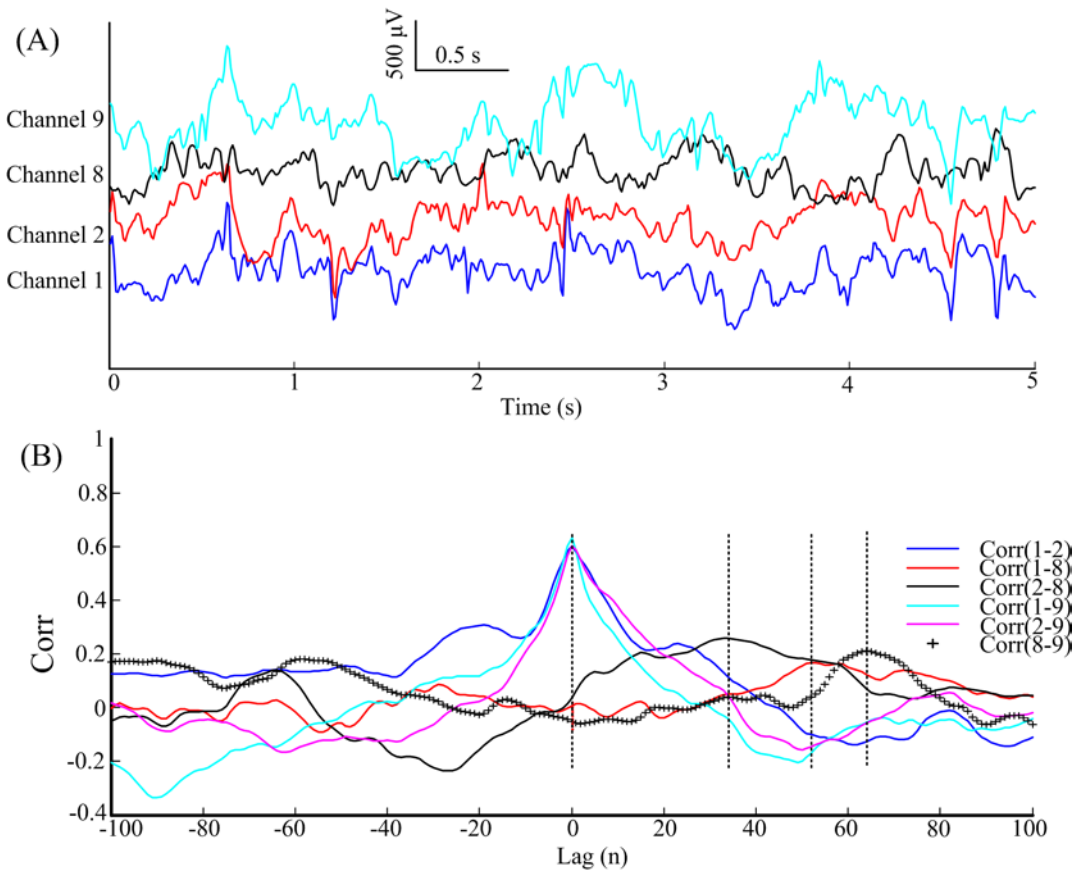

Figure S13. Lag analysis of four channels from the same subject as in Figure 4 in unconscious state.

There are two main methods to reduce the influence of volume conduction effects on the brain network assessment. One is to solve the inverse problem and to estimate the brain network among the brain sources [33,34]. However, using the inverse solution to find the brain source is an ill-posed problem due to the finite number of sensors and the unknown number of the sources [34]. This makes it difficult to have an accurate estimation of the connectivity based on the sources. The other is to is to develop measures that are " robust to volume conduction artifact" [29]. Several brain connectivity measures have been proposed to provide a robust ability to withstand instantaneous linear mixing (the nature of the volume conduction artifacts), such as the phase lag index [35], the weight phase lag index [36], the imaginary part of coherency [37], and the direct phase lag index [38]. In the study of [20], the authors proposed a measure named weight symbolic mutual information (wSMI) to qualify the consciousness in noncommunicative patients. Working in a similar way to the PCMI measure, the wSMI has the virtue of being able to disregard the conjunctions of identical and opposite-sign symbols. All this makes the wSMI measure able to eliminate the influence of the common-source artifact, which is potentially associated with volume conduction effects.

Generally speaking, the ECoG method records neural activities directly from the cortical surface, which is not influenced by the spatial distribution of brain sources from the layers of dura, scalp, and skull. Most ECoG studies didn't take into account volume conduction effects in measuring the cortical networks [39-41]. Some other researchers suggested considering volume conduction effects in ECoG studies. However, compared with scalp EEG and MEG recordings, studies on the source-reconstruction of ECoG signals have been inadequate [32]. Fischer et al. used

envelope intrinsic coupling modes method, which is free from the influence of zero-phase lagged components, to eliminate volume conduction effects [42]. The studies of [21] and [30] employed the independent component analysis (ICA) method as a spatial-temporal filter to solve the volume conduction problem in ECoG signals. Hindriks et al. suggested using the source-space spatial ICA method to identify generators of cortical rhythms and to reconstruct functional connectivity [32]. All these studies have paved the way for the use of the ICA method to overcome volume conduction effects.

In order to analyze volume conduction effects in ECoG signals, we took the following actions: (1) We used the ICA method to test whether the ECoG channels, which are highly correlated with each other (correlation coefficient greater than 0.5), derive from the same sources. (2) We analyzed whether the short-distance electrodes with small lags (less than 10 ms) derive from the same sources.

We want to analyze the communication between ECoG channels in different distances and cortical regions, so it is important to obtain the potential of the source on the cortical surface. In this study, we considered two methods to eliminate volume conduction effects. One is the current source density (CSD) transform, which can diminish volume conduction effects and estimate the potential of the source on the cortical surface [20]. The CSD toolbox was used to calculate the potential of the ECoG. The other one is the ICA-based method proposed in the study [21]. The performance of these two methods was analyzed. We also calculated the wSMI values, which has been proven to be effective in diminishing volume conduction effects arising from the common-source artifact in EEG sale. More detailed analyses are provided in the following sections.

3.1 Correlation analysis and source calculation based on independent component analysis

To decompose ECoG signals into equal numbers of independent signals, we used the FastICA algorithm (a publicly available software, FastICA v2.5 (http://www.cis.hut.fi/projects/ica/fastica/), which functions similarly to the ICA method based on an “infomax” neural network. To verify whether channels with low lags (less than 10 ms with the correlation coefficient greater than 0.5) derive from the same source, we calculated the independent component (IC) of all channels using the ICA method. The ICs’ contribution to channel signals was quantified by the percent variance accounted for (PVAF) [21]. From the mathematical point of view, considered the signal $Xi(t)$ of channel i and the component j, the component j back-projection on channel i is defined as:

$$Xj,i(t) = Wj,i(-1) * S_j(t) \tag{4}$$

Where $W(-1)$ is the mixing matrix of ICA and $S_j(t)$ represents the activation time series of component *j*. The PVAF of component j to channel i is:

$$PVAF_{j,i} = \left[1 - \frac{\mathrm{var}(X_i(t) - X_{j,i}(t))}{\mathrm{var}(X_i(t))}\right] * 100 \quad (5)$$

The lag matrixes of all paired-channels with the epoch lengths of 10 s and 350 s (the epoch length of this subject in wakeful and unconscious states is about 350 s) and during the entire time course are shown in Figure S14. There are a larger number of near-zero-lag paired-channels (black points) in wakeful state than in unconscious state. The percent values of near-zero-lag (less than 10 ms) as well as highly correlated paired-channels are shown in Table S2.

Also, for all these highly correlated paired-channels, the percent of different electrodes distances were presented in table S3. Only 12.8% of the near-zero-lag paired-channels in wakeful state derive from sources with an electrode distance of 1 cm when the epoch length is 10 s. Near-zero-lag paired-channels deriving from sources with an electrode distance of greater than 7 cm account for more than 20% of the total for this subject. This indicates that the high linear correlation is not highly related with the electrode distance. However, the percent of near-zero-lag paired-channels deriving from sources with a short electrode distance (less than 2 cm) is higher in unconscious state than in wakeful state for this subject.

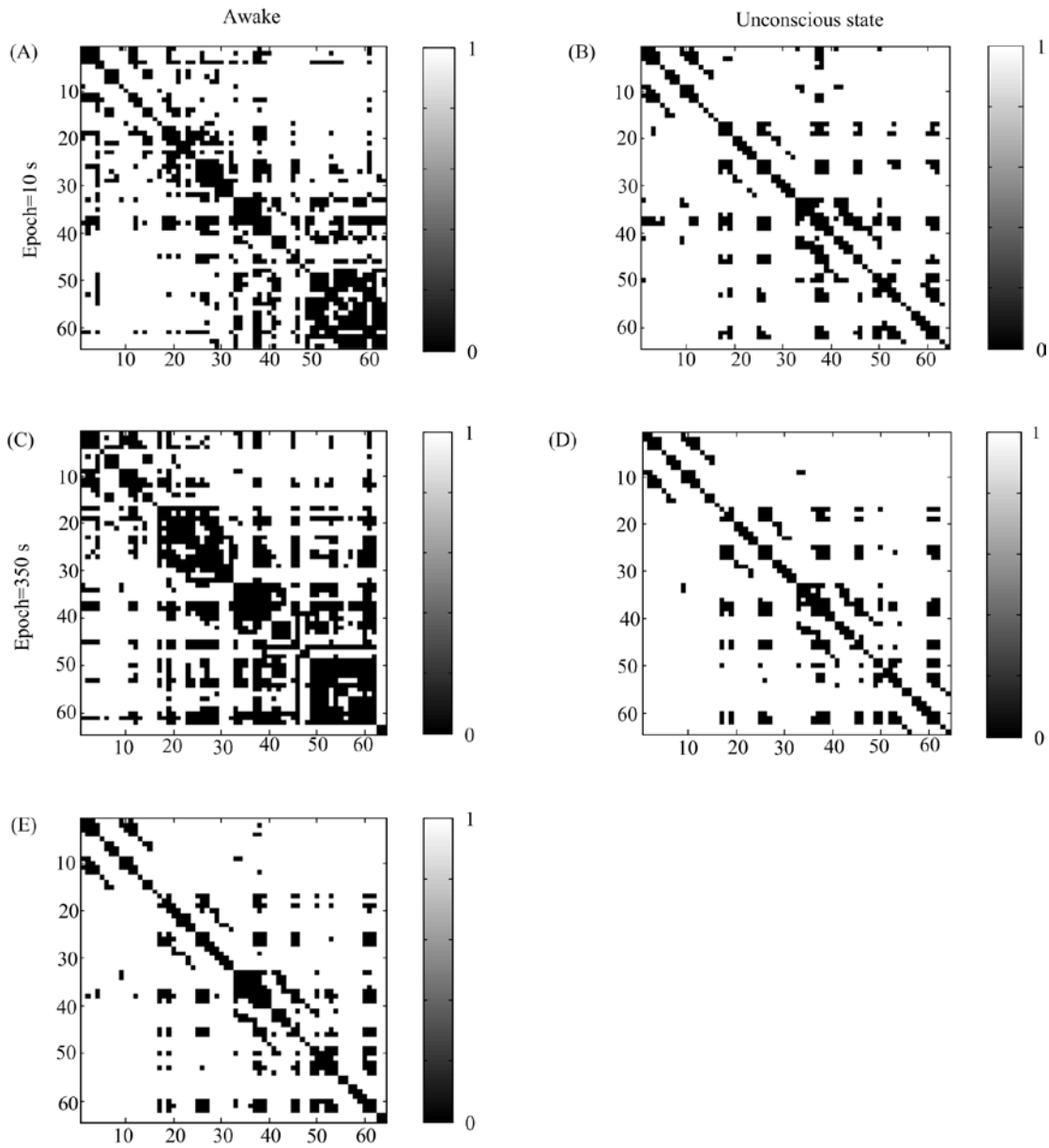

Figure S14. The lag matrixes of all channels in wakeful and unconscious states. The black points denote channels with a lag of less than 10 ms under the correlation coefficient of greater than 0.5. The white points denote channels with a lag of greater than 10 ms and a correlation coefficient less than 0.5. (A) and (B): The lag matrixes in wakeful and unconscious states, respectively, when the epoch length is 10 s. (C) and (D): The lag matrixes when the epoch length is 350 s. (E): The lag matrix of all channels during the entire time course.

Table S2. The percent values of near-zero-lag (less than 10 ms) paired-channels in different epoch lengths.

	Epoch=10 s (N=2016)	Epoch=350 s(N=2016)	Epoch=700 s(N=2016)
WS	22.47 %	31.05 %	
US	11.66 %	10.07 %	
Entire time course			11.56 %

WS: wakeful state
US: unconscious state

Table S3. The percent values of highly correlated (lag < 10 ms with the correlation coefficient > 0.5) paired-channels in different electrode distances.

	1 cm	2 cm	3 cm	4 cm	5 cm	6 cm	7 cm	>7 cm
WS, 10 s	12.80%	13.25%	7.06%	7.73%	5.74%	10.82%	11.48%	31.12%
US, 10s	23.83%	14.47%	3.40%	5.96%	3.83%	11.60%	16.17%	20.74%
WS, 350 s	10.06%	11.34%	7.83%	7.99%	5.27%	10.22%	14.06%	33.23%
US, 350 s	26.11%	15.27%	3.45%	5.42%	5.42%	9.85%	13.30%	21.18%
Entire time course	24.46%	15.02%	5.15%	5.15%	5.15%	9.01%	14.60%	21.47%

IC calculations based on the data in Figure S14 are shown in Figures S15, S16, and S17. We analyzed the first three maximal ICs of the paired-channels based on their weight values (PVAF). Figure S15 shows the paired-channels deriving from the same first, first two, and first three maximal ICs in wakeful and unconscious states. The data length of the analyzed ECoG data is 10 s, same as in Figure S14 (A) and (B). The percent values of paired-channels deriving from the various sources in an epoch length of 10 s, 350 s, and during the entire time course are shown in Table S4. IC calculation based on the entire time course shows that about 10.27% paired-channels derive from the same first maximal IC

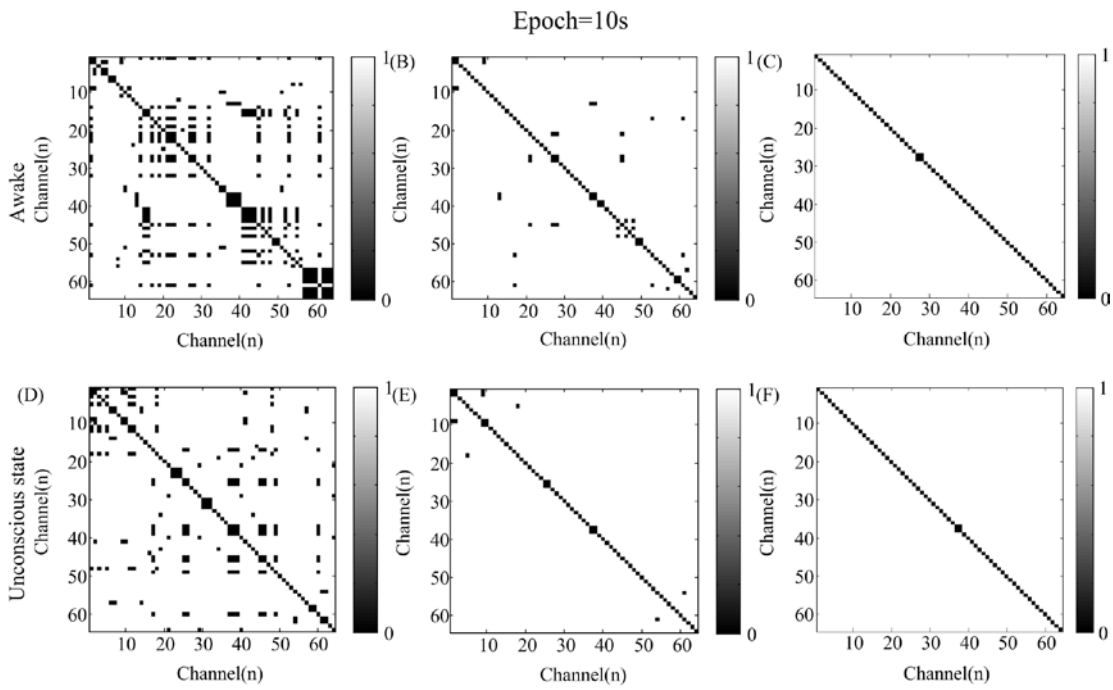

Figure S15. Analysis of common source paired-channels (denoted in black points) of one subject in awake and unconscious states when the epoch length is 10 s. (A)-(C): Matrixes of paired-channels deriving from the same first, first two, and first three maximal ICs, respectively, in wakeful state. (D)-(F): Matrixes of paired-channels deriving from the same first, first two, and first three maximal ICs, respectively, in unconscious state.

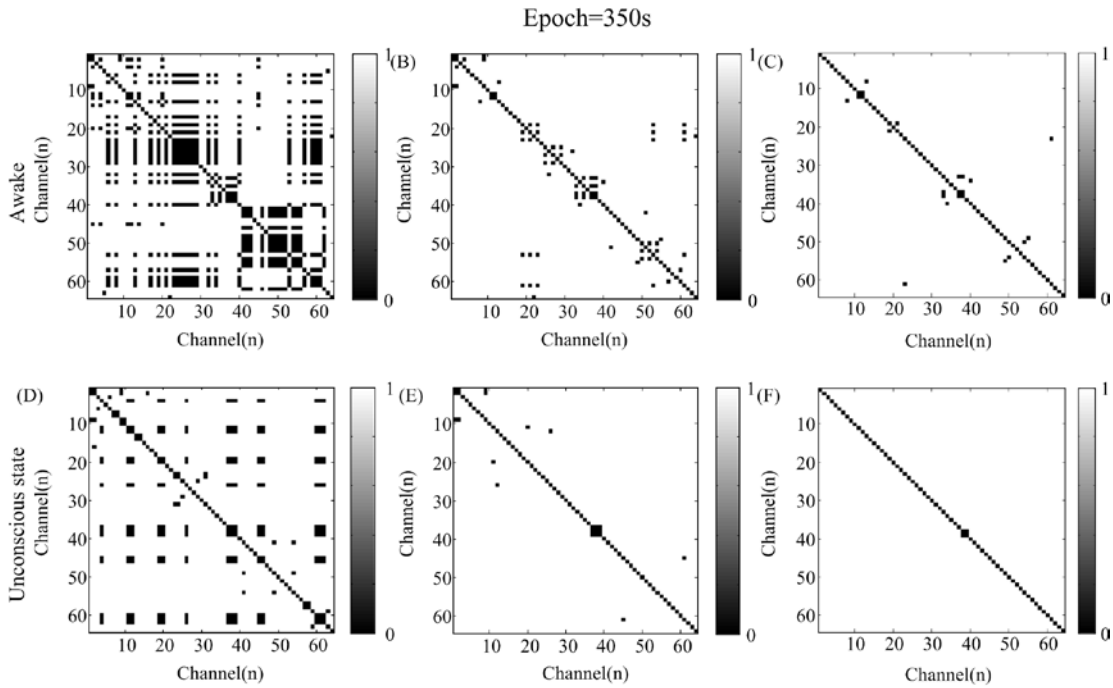

Figure S16. Analysis of common source paired-channels (denoted in black points) of one subject in wakeful and unconscious states when the epoch length is 350 s. (A)-(C): Matrixes of paired-channels deriving from the same first, first two, and first three maximal ICs, respectively, in wakeful state. (D)-(F): Matrixes of paired-channels deriving from the same first, first two, and first three maximal ICs, respectively, in unconscious state.

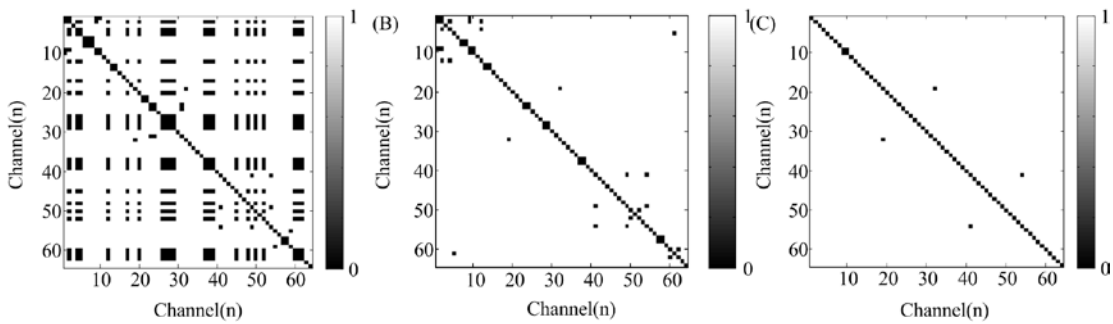

Figure S17. Analysis of common source paired-channels (denoted in black points) during the entire time course. (A)-(C): Matrixes of paired-channels deriving from the same first, first two, and first three maximal ICs, respectively, during the entire time course.

Table S4. The percent values of common sources with different epoch lengths in wakeful and unconscious states.

	First maximal IC	First two maximal ICs	First three maximal ICs
WS, epoch= 10s	8.48%	0.94%	0.04%
US, epoch= 10s	4.86%	0.25%	0.04%
WS, epoch= 350s	15.92%	1.54%	0.50%

US, epoch= 350s	5.21%	0.84%	0.04%
Entire time course	10.27%	0.84%	0.15%

For the common source paired-channels, we need to verify whether they have a lag of less than 10 ms and a correlation coefficient of greater than 0.5. For the near-zero-lag paired-channels, however, it is crucial to examine whether they derive from common sources. Table S5 shows the percent of near-zero-lag paired-channels (correlation coefficient > 0.5) in all the common source paired-channels. The numbers of common source paired-channels in all near-zero-lag and highly correlated paired-channels are shown in Table S6. It can be seen that paired-channels deriving from the same sources tend to have a high correlation coefficient and a low lag. Almost all the paired-channels deriving from the same first three maximal ICs have a high correlation coefficient and a low lag. This means that channels deriving from the same source tend to have a high correlation coefficient and a low lag. Table S6 shows that among all the channels with a low lag and a high correlation coefficient, only 40% of them derive from the same source. This means that highly correlated channels do not necessarily derive from the same source, and common source paired-channels tend to be more correlated with each other.

Table S5. The percent values of near-zero-lag paired-channels in all the common source paired-channels.

	First maximal IC	First two maximal ICs	First three maximal ICs
WS, epoch= 10s	166/342=48.54%	28/38=73.68%	2/2=100%
US, epoch= 10s	114/196=58.16%	8/10=80%	2/2=100%
WS, epoch= 350s	406/642=63.24%	56/62=90.32%	18/20=90%
US, epoch= 350s	112/210=53.33%	8/12=66.67%	2/2=100%
Entire time course	166/414=40.10%	28/34=82.35%	4/6=66.67%

Take the epoch length of 10 s for instance. 166/342 means that among the 342 paired-channels driving from the same first maximal IC, 166 have a high correlation coefficient (>0.5) and a low lag (less than 10 ms).

Table S6. The percent values of paired-channels deriving from the same source in all near-zero-lag (less than 10 ms) paired-channels.

	First maximal IC	First two maximal ICs	First three maximal ICs
WS, epoch= 10s	166/906=18.32%	28/906=3.09%	2/906=0.22%
US, epoch=	114/470=24.26%	8/470=1.70%	2/470=0.43%

10s			
WS, epoch= 350s	406/1252=32.43%	56/1252=4.47%	18/1256=1.44%
US, epoch= 350s	112/406=27.59%	8/406=1.97%	2/406=0.49%
Entire time course	166/466=35.62%	28/466=6.01%	4/466=0.86%

Take the epoch length of 10 s again for instance. 166/906 means that among the 906 paired-channels with a high correlation coefficient (>0.5) and a low lag (< 10 ms), 166 derive from the same first maximal IC.

3.2. Analysis of the current source density and independent component analysis methods for volume conduction effects elimination

For the CSD transform, we employed the CSD toolbox for calculation [43]. Figure S18 shows the ECoG signals from two channels after the CSD transform. The correlation coefficient (R) between the two channels of signals reaches 0.97 and the signals are almost identical across the two channels. This indicates that the CSD transform increases the linear similarity between signals from different channels.

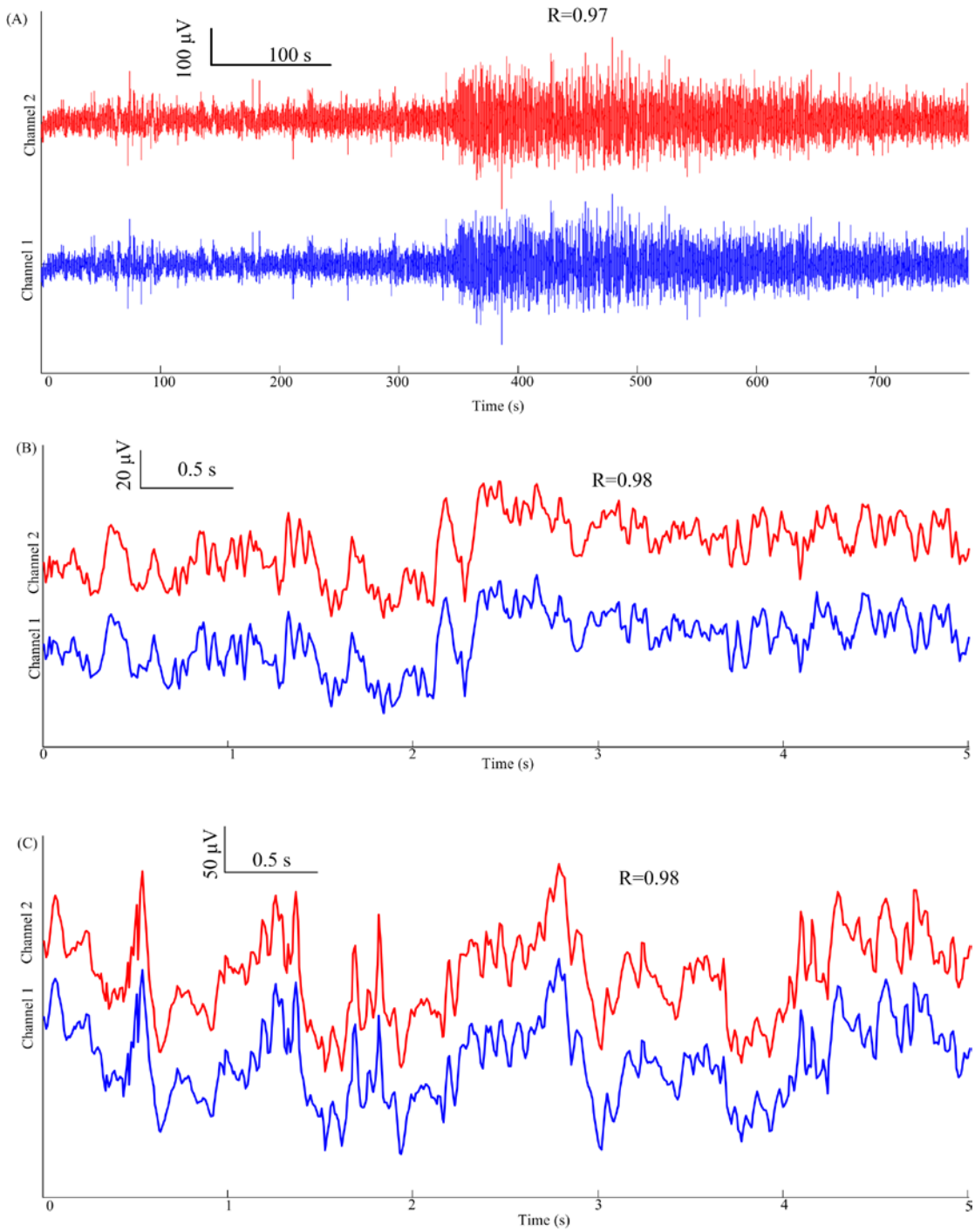

Figure S18. The ECoG recordings of Channels 1 and 2 after the CSD transform. (A): The two channels of ECoG signals over the entire time course. (B) and (C): The ECoG signals of 5 seconds in awake and unconscious states, respectively.

The common source evaluation of CSD transformed ECoG was made using the ICA method. The common source channels with the first maximal IC, the first two maximal ICs, and the first three maximal ICs are shown in Figure S19. It can be seen that the number of paired-channels with the first maximal IC increases after ECoG is CSD transformed. It is worth noting that the almost all the common source paired-channels fall within the same strip (electrodes 1 to 16 are in strip 1, 17 to 32 in strip 2, 33-48 in strip 3, and 49-64 in strip 4) and no common source exists

between two channels in different strips. This indicates that the CSD enhances the linear similarity between channels in the same strip. So, the CSD does not effectively eliminate the impact of volume conduction on ECoG data in this study.

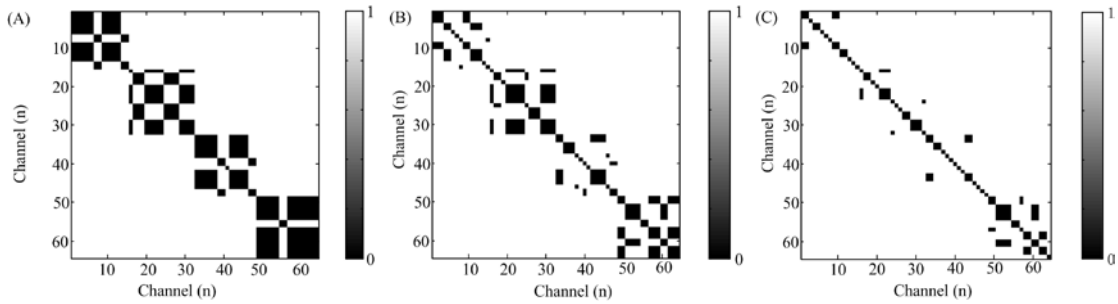

Figure S19. The common source paired-channels after the CSD transform in the awake state. (A): Common source paired-channels (denoted in black points) deriving from the same first maximal IC. (B) and (C): Common sourcepaired-channels deriving from the same first two and first three maximal ICs, respectively.

For the ICA-based method, the study of [21] used four independent components to replace the original signals. The squared Pearson's correlation (R^2) was employed to quantify the strength of the linear dependence between two variables. When the correlation decreases, it means that the similarity between two time series is reduced. A lower R^2 value means that the time series are more independent from each other. $R^2 = 0.5$ was considered an important threshold for evaluating the linear dependence in the study of [21].

In this study, we employed a similar method to attenuate the influence of volume conduction effects. The procedure is described as follows:

(1) The original ECoG signals of 64 channels were decomposed using the FastICA method.

(2) Weights of the ICs were calculated for each channel using the PVAF method.

(3) In the case of two ECoG signals, we used the ICs to replace the original signals. Channels having three common sources in their first five maximal ICs were regarded as ones deriving from the same sources.

(4) To calculated the PCMI, the signals of paired-channels deriving from common sources were replaced by their first five maximal ICs except the common sources. Paired-channels deriving from two or less of the first five maximal ICs were calculated using the original signals.

Based on the above procedure, the original ECoG signals were decomposed into equal numbers of ICs (N=64). A 10-second segment of signals from Channel 2 with the same patient as in Figure 4 and its ICs are shown in Figure S20. To evaluate the performance of the ICA and CSD methods in eliminating volume conduction effects, we calculated the R^2 values of the original ECoG signals and the signals after the ICA-based procedure and the CSD transform. We only analyzed the R^2 values with the *p*-value less than 0.05. The results show that the R^2 values of paired-channels with replaced ICs are much smaller than those of the original signals (see Figure S21). Whereas, the R^2 values of some signals after the CSD transform are greater than 0.5, even close to 1. This indicates that the CSD transform enhances the linear similarity between the ECoG signals. Hence, compared to the ICA method, the CSD transform is a less-than-optimal method to

eliminate volume conduction effects for ECoG signal analysis. Therefore, we selected the ICA method for volume conduction effect elimination.

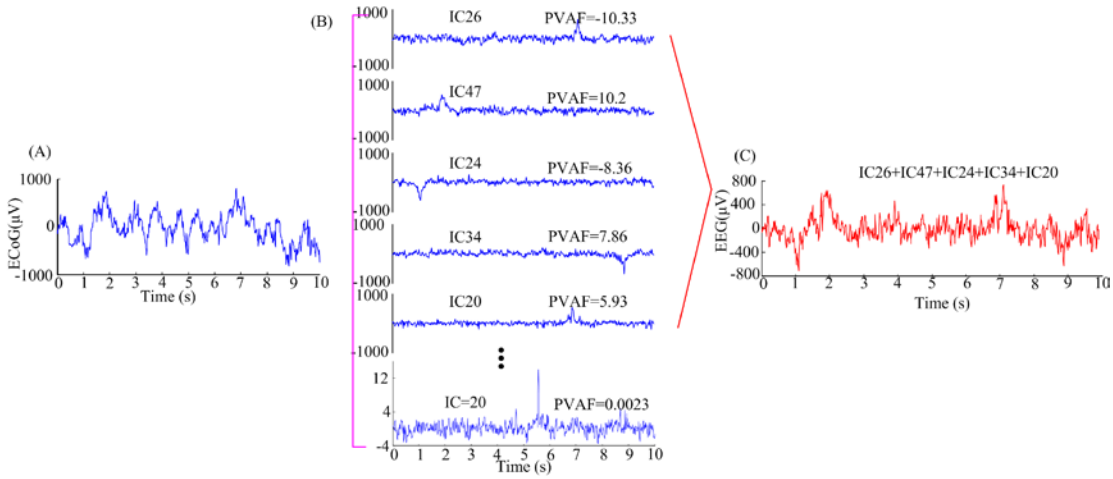

Figure S20. Decomposition of ECoG signals using the ICA method. (A) Original signals in an epoch length of 10 s. (B) The ICs of the signals. The weight of the ICs to the ECoG signals reduce from top to bottom. (C) The sum of the signals of IC26, IC47, IC24, IC34, and IC20.

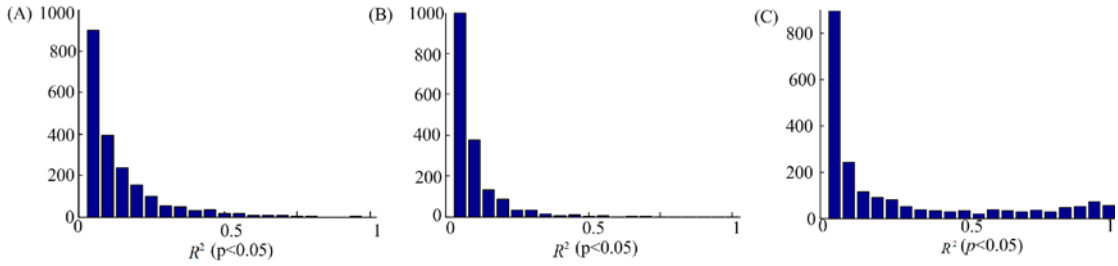

Figure S21. The R^2 distribution of the channels with all lengths of time. (A)-(C): The R^2 values of original ECoG signals, signals after the ICA-based procedure, and signals after the CSD transform, respectively.

Based on the abovementioned ICA-based procedure for volume conduction effect elimination, we calculated the PCMI values of the same channels (Channels 1, 2, 8, and 9) as in Figure 4. The results show that all the PCMI values decrease after the loss of consciousness (see Figure S22). The PCMI values with short-distance electrodes (1 and 2, 1 and 9, 2 and 9) exhibit a decrease trend in unconscious state, significantly different from those of original ECoG channels. As shown in Figure S16, Channels 1 and 2, 1 and 9, as well as 2 and 9 share the common sources in their first maximal IC. The PCMI values decrease after the ICA-based procedure. This means that volume conduction may have a major effect on the increasing PCMI values with short-distance electrodes, and this effect can definitely be reduced by using the ICA method. It can be seen that the information integration decreases in both the local range and the long distance. Therefore, the conclusion that the information integration increases in the local range was incorrect. The volume conduction effects led us to a wrong conclusion.

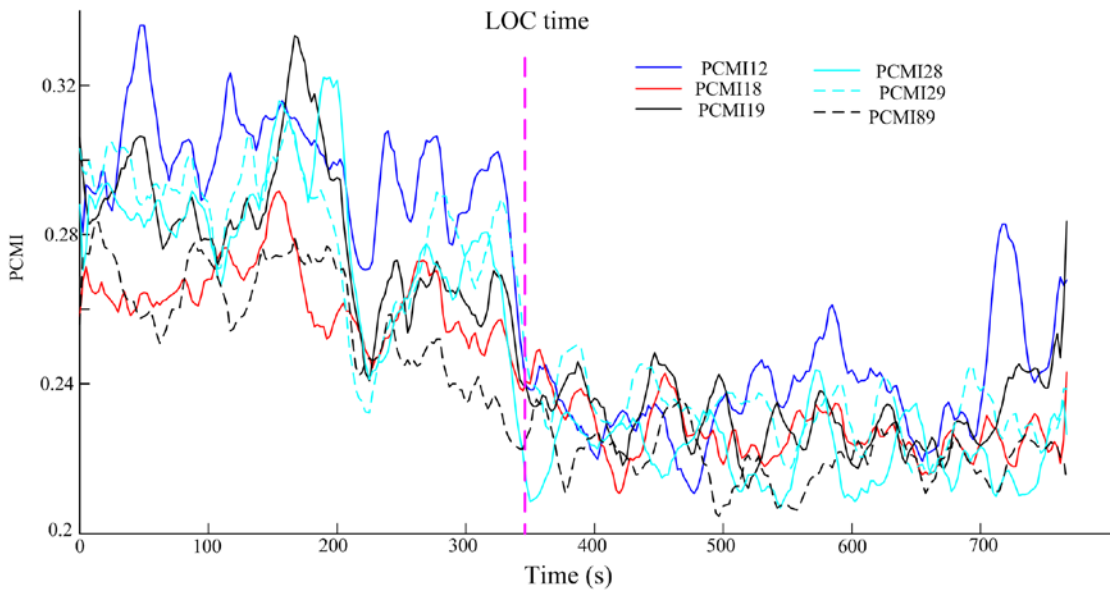

Figure S22. The PCMI values of the same subject as in Figure 4 based on the ICA method. PCMI12 represents the PCMI value of channels 1 and 2, and so on.

3.3. Analysis of ECoG signals based on the weight symbolic mutual information values.

We also calculated the wSMI values for comparison. The wSMI of original ECoG signals and ECoG signals after the ICA-based procedure are shown in Figure S22. The same data as in Figure 4 was analyzed and the parameters for the wSMI were set as $m = 4$, $\tau = 2$, and epoch= 6 s. The results show that the wSMI values of original ECoG signals of short-distance channels increase after LOC (see Figure S23 (A)), whereas those of ECoG signals after the ICA-based procedure decrease after LOC (see Figure S23 (B)). However, the wSMI values of ICA-based ECoG signals in wakeful state demonstrate larger variations than those of original ECoG signals. We further analyzed the wSMI values of original ECoG signals and ECoG signals after the ICA-based procedure with a “linear surface distance” of 1 cm and 6 cm, respectively, for all subjects. The results show that the wSMI values of original ECoG signals increase in unconscious state, whereas those of ECoG signals after the ICA-based procedure decrease in both 1 cm and 6 cm. Therefore, we considered the ICA-based procedure combined with wSMI a more effective method than wSMI alone in terms of eliminating volume conduction effects.

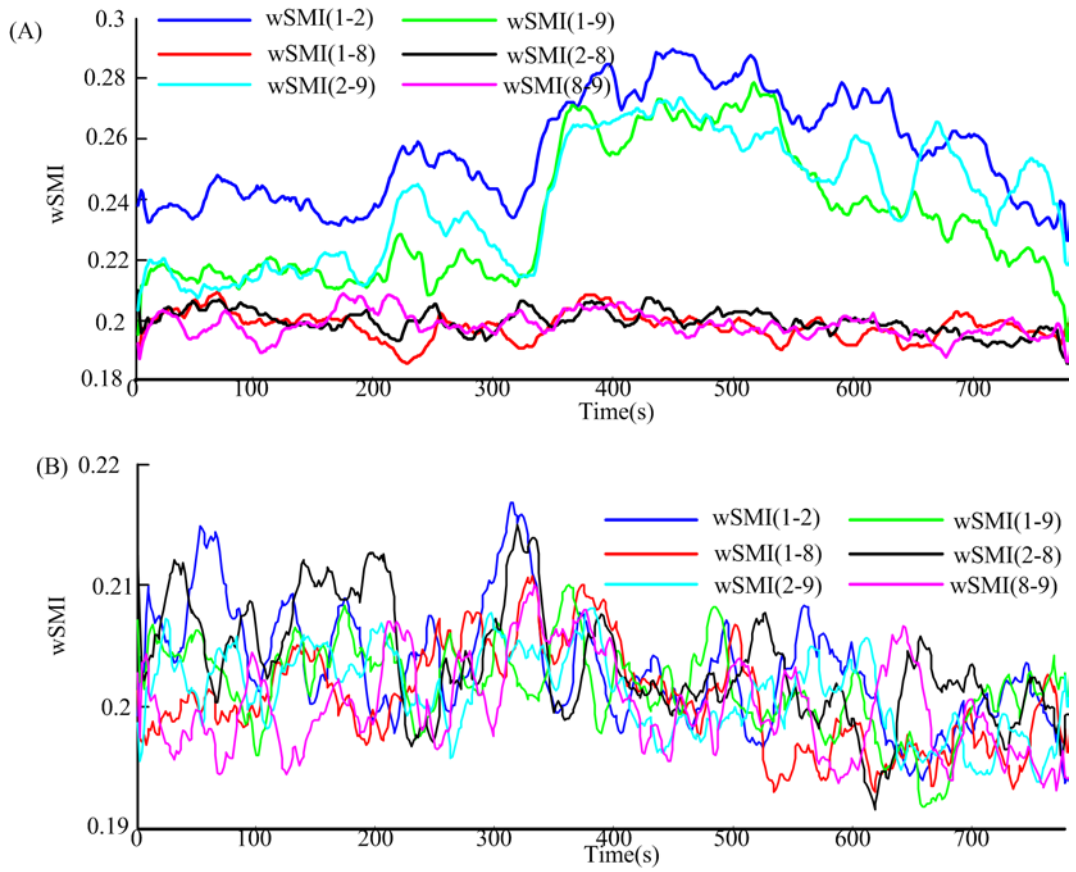

Figure S23. The wSMI values of original ECoG signals (A) and ECoG signals after the ICA-based procedure (B).

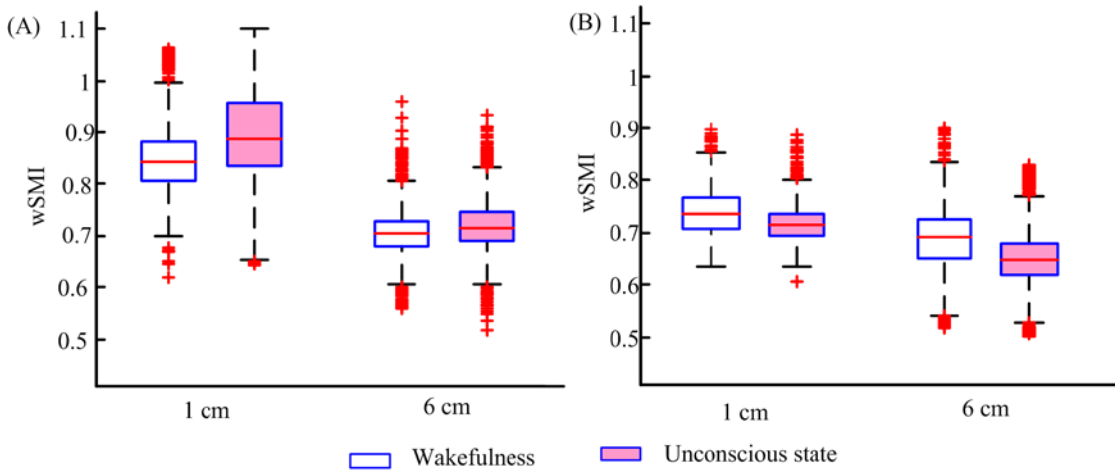

Figure S24.The wSMI values of original ECoG signals (A) and ECoG signals after the ICA-based procedure (B) with an electrode distance of 1 cm and 6 cm, respectively.

Part 4. Power spectrum analysis of ECoG signals

Considering the significant amplitude increase after LOC in all these four channels, we analyzed the spectrum of all channels in this subject. The average power and the spectrum during the time course are shown in Figure S25. It can be seen that the power in the 0.5-45 Hz frequency band increases in unconscious state, which is especially so when the frequency is less than 5 Hz.

We also analyzed the relative power spectrum density (RPSD) of the five frequency bands: 1) delta (0.1-4 Hz), 2) theta (4-8 Hz), 3) alpha (8-13 Hz), 4) beta (13-30 Hz), and 5) gamma (30-47 Hz). The RPSD is calculated by:

$$RPSD(f_1, f_2) = \frac{p(f_1, f_2)}{p(0.1,47)} \tag{6}$$

Where $RPSD(\cdot)$ is the relative power spectral density with the frequency band of f_1 and f_2; $p(\cdot)$ is the power that is computed using the *pwelch* method; and $p(0.1,47)$ is the power in the 0.1-47 Hz frequency band. The RPSD values in the delta, theta, alpha, beta, and gamma frequency bands are represented as RPSD (delta), RPSD (theta), RPSD (alpha), RPSD (beta), and RPSD (gamma).

Figure S26 (C)-(F) show that the RPSD values in delta (mainly related with the amplitude) increase after LOC. But the RPSD values in awake state are instable in all four channels. Therefore, it is hard to say whether the effect concentration can be tracked with the amplitude.

In the section of Part 3, we analyzed the lag and the correlation coefficient of these four channels. The results show that the lag values in near distances (electrodes 1-2, 1-9, and 2-9) are smaller than those in long distance. Also, analysis by the ICA method shows that the paired-channels with short lags (less than 10 ms) are more likely to derive from the same sources (due to the volume conduction effects). Based on the signals reconstructed from ICs, we found that the PCMI value decreases after LOC in short-distance electrodes (see Figure S21). This demonstrates that volume conduction may be the cause of increasing PCMI values between short-distance electrodes.

The PCMI is derived by utilizing symbolic dynamics and mutual information. The symbolic dynamic analysis is performed mainly by discretizing the time-series into a corresponding sequence of symbols by comparing neighboring time points [15]. Therefore, it is more related to the relative amplitude of the signal than to the amplitude itself. We still believe that it is the PCMI, instead of the magnitude, that reflects the changes in information integration.

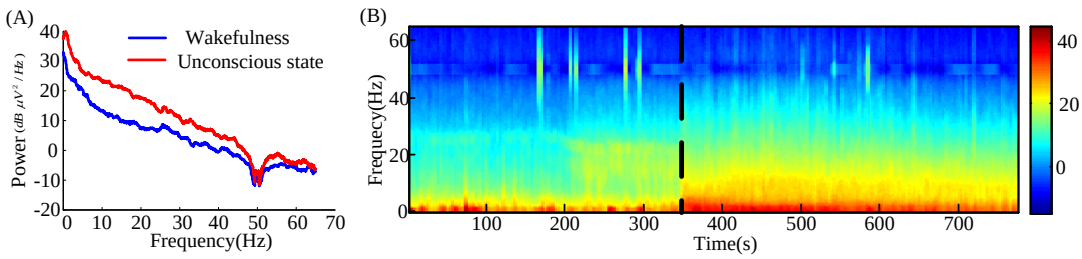

Figure S25. (A)The average power in awake and unconscious states. (B) The average power spectrogram across all electrodes from one subject.

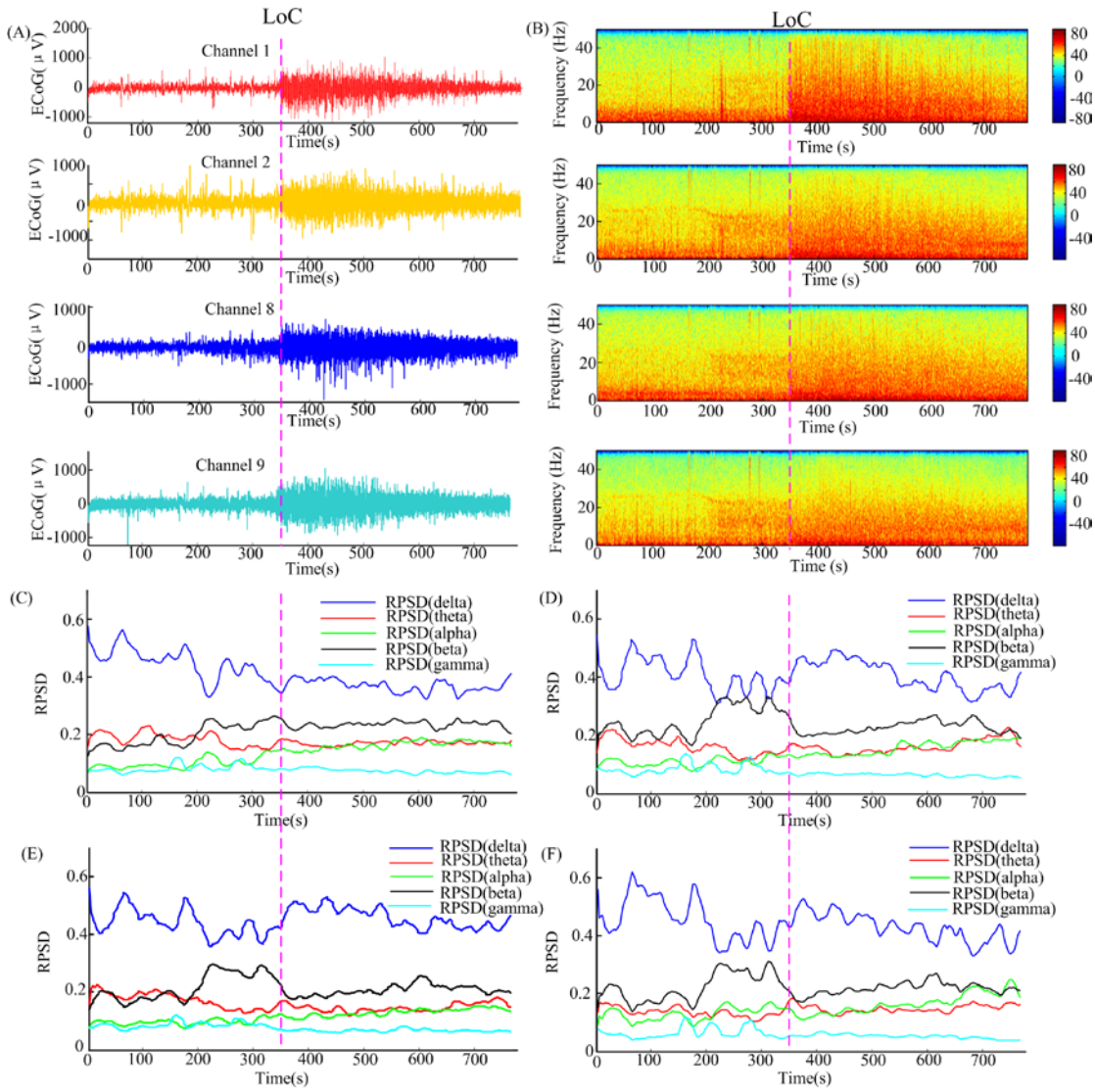

Figure S26. (A) and (B): The ECoG waveforms of the same subject as in Figure 4 and their corresponding spectrograms. The spectrograms were computed via the short-time Fourier transform and windowed with a Hamming window. The epoch of the calculation is 10 s with 75% overlapping. (C)-(F): The RPSD values in five sub-bands versus time for ECoG signals of Channels 1, 2, 8, and 9.

Interestingly, a consistent beta activity appears approximately 150 sec before LOC for this subject. The study of [44] showed that, in EEG scale, the beta power increased in frontal/central area in light sedation during propofol anesthesia. In deep sedation, alpha oscillation dominated in frontal area. With loss of consciousness, slow wave oscillations (delta and theta power) increased in frontal area. However, we have re-checked the time point of the drug induction under the help of the anesthesiologist, and it was found that not all the patients had obvious beta oscillation before the LOC. As seen in the following figure S27, there was no consistent sustained beta wave phenomenon before the time point of LOC.

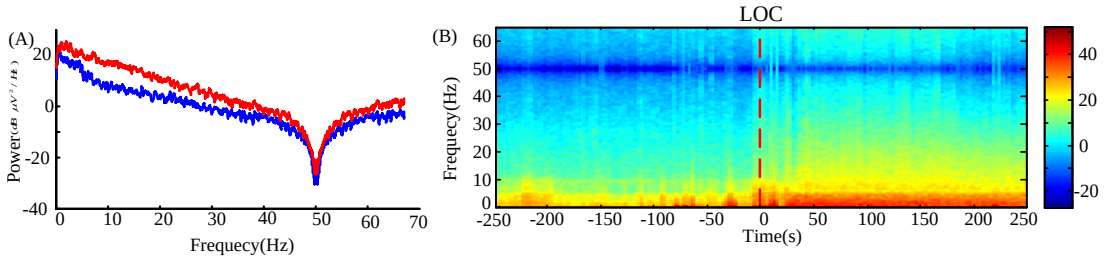

Figure S27. (A) The average power in awake and unconscious states. (B) The average power spectrogram across all electrodes from one subject during the time range from LOC-250 (the time point of 250 s before LOC) to LOC+250 (the time point of 250 s after LOC).

Part 5. Surrogate data analysis based on the total space of data

In order to compare analytical results of single channel surrogate data and the total space of data, we also analyzed the GPCMI values based on the surrogate data of 64 channels. Figure S28 shows the GPCMI values of the same ECoG signals as in Figure 4, which were measured across the total space through the ICA-based procedure. The surrogate data were selected from all channels (10 for each channel). The results show a higher percent of non-zero GPCMI values than the single electrode based measure.

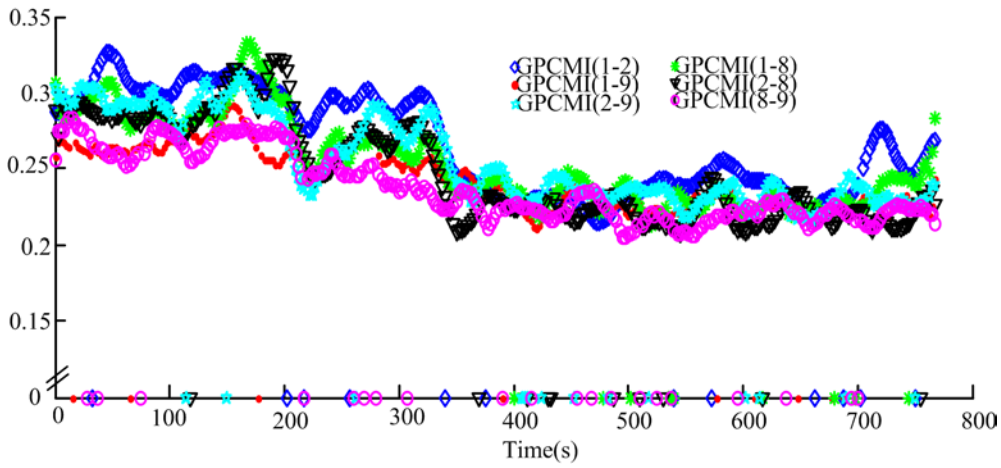

Figure S28. The GPCMI values of electrodes 1, 2, 8, and 9, based on the surrogate data.

Part 6. Single frontal region cannot distinguish different state of conscious with different anesthetic agents

This study found that the N-GPCMI decreased in the frontal region after LOC (figure 6A). Recently, in the study of [45], the authors proposed that frontal montage is uninformative regarding DoA. However, this argument does not conflict with our current results. First, in the study of [45], they employed the BIS as an index for consciousness assessment, which derived from one channel EEG. Most of studies have showed that the connections between different brain regions (i.e., frontoparietal connectivity) are more related with consciousness [11,28,46,47]. Nowadays, the BIS

Vista-Bilateral Monitoring System (Anadic medical systems INC), supplied 4 channel EEG recording for a more reliable consciousness assessment. Also, the product of SEDLine brain function monitoring (Masimo corporation) employed the similar design to collect the EEG signal from two sides of prefrontal areas and generate an index to measure the depth of anesthesia [48]. Second, except from the frontal region, in other regions (i.e., temporal and parietal), as well as the cortical regions among T-P also had significant difference between wakefulness and unconscious state ($p<0.001$ in all these regions or region-pairs). Since the number of patients with electrodes in frontal region was less than 5, we haven't make statistics for frontal region. It indicated that the propofol induced unconsciousness lead to a reduction of information integration across the cortex based on the measure of PCMI. Thirdly, Blain-Moraes et al. found that the phase amplitude coupling between low-frequency phase and alpha amplitude haven't emerged in the frontal cortex in sevoflurane, which is an obvious characteristics in propofol [49]. They suggested that the phase-amplitude coupling in the parietal region and phase lag index across cortex are more reliable markers to measure the sevoflurane-induced unconsciousness. These studies indicated that different anesthetic may need different measure and the evaluation of the coupling or connection across regions should be a more general biomarker for clinical practice. Finally, in the study of [45], there are only two subjects, they are all old age patients (> 72 years old) and the first one sustained severe prefrontal cortical injury as an adolescent. Purdon et al. found that the amplitude of EEG oscillations in elderly patients is about 2 to 3 fold smaller than that in younger adults in propofol and sevoflurane induced anesthesia. Especially, the alpha band showed a specific age-related changes [50]. The EEG characteristics during anesthesia in infants [51] and children [52] have also been proved to be age-related. However, the commercial EEG-based DoA system haven't considered the effect of the age. Therefore, the frontal montage may also not the only reason to the uninformative monitoring in DoA. The age-related, anesthetics-related investigation should be considered in future study.

References

1. Schreiber T, Schmitz A: Improved Surrogate Data for Nonlinearity Tests. Phys Rev Lett 1996; 77: 635-638
2. Cui D, Liu X, Wan Y, Li X: Estimation of genuine and random synchronization in multivariate neural series. Neural Netw 2010; 23: 698-704
3. David O, Cosmelli D, Friston KJ: Evaluation of different measures of functional connectivity using a neural mass model. Neuroimage 2004; 21: 659-673
4. Schellenberger Costa M, Weigenand A, Ngo HV, Marshall L, Born J, Martinetz T, Claussen JC: A Thalamocortical Neural Mass Model of the EEG during NREM Sleep and Its Response to Auditory Stimulation. PLoS Comput Biol 2016; 12: e1005022
5. Nevado-Holgado AJ, Marten F, Richardson MP, Terry JR: Characterising the dynamics of EEG waveforms as the path through parameter space of a neural mass model: application to epilepsy seizure evolution. Neuroimage 2012; 59: 2374-92
6. Liang Z, Duan X, Su C, Voss L, Sleigh J, Li X: A Pharmacokinetics-Neural Mass Model (PK-NMM) for the Simulation of EEG Activity during Propofol Anesthesia. PLoS One 2015; 10:

e0145959
7. Wendling F, Bellanger JJ, Bartolomei F, Chauvel P: Relevance of nonlinear lumped-parameter models in the analysis of depth-EEG epileptic signals. Biol Cybern 2000; 83: 367-78
8. Li X, Ouyang G: Estimating coupling direction between neuronal populations with permutation conditional mutual information. Neuroimage 2010; 52: 497-507
9. David O, Friston KJ: A neural mass model for MEG/EEG: coupling and neuronal dynamics. Neuroimage 2003; 20: 1743-55
10. Williams ML, Sleigh JW: Auditory recall and response to command during recovery from propofol anaesthesia. Anaesth Intensive Care 1999; 27: 265-8
11. Liang Z, Ren Y, Yan J, Li D, Voss LJ, Sleigh JW, Li X: A comparison of different synchronization measures in electroencephalogram during propofol anesthesia. J Clin Monit Comput 2016; 30: 451-66
12. Trongnetrpunya A, Nandi B, Kang D, Kocsis B, Schroeder CE, Ding M: Assessing Granger Causality in Electrophysiological Data: Removing the Adverse Effects of Common Signals via Bipolar Derivations. Front Syst Neurosci 2015; 9: 189
13. Fatourechi M, Bashashati A, Ward RK, Birch GE: EMG and EOG artifacts in brain computer interface systems: A survey. Clin Neurophysiol 2007; 118: 480-94
14. Liang Z, Liang S, Wang Y, Ouyang G, Li X: Tracking the coupling of two electroencephalogram series in the isoflurane and remifentanil anesthesia. Clin Neurophysiol 2015; 126: 412-22
15. Bandt C, Pompe B: Permutation entropy: a natural complexity measure for time series. Phys Rev Lett 2002; 88: 174102
16. Shelhamer M: Nonlinear dynamics in physiology: a state-space approach, World Scientific, 2007
17. Liang Z, Wang Y, Sun X, Li D, Voss LJ, Sleigh JW, Hagihira S, Li X: EEG entropy measures in anesthesia. Front Comput Neurosci 2015; 9: 16
18. Kreuz T, Mormann F, Andrzejak RG, Kraskov A, Lehnertz K, Grassberger P: Measuring synchronization in coupled model systems: A comparison of different approaches. Physica D: Nonlinear Phenomena 2007; 225: 29-42
19. Olofsen E, Sleigh JW, Dahan A: Permutation entropy of the electroencephalogram: a measure of anaesthetic drug effect. Br J Anaesth 2008; 101: 810-21
20. King JR, Sitt JD, Faugeras F, Rohaut B, El Karoui I, Cohen L, Naccache L, Dehaene S: Information sharing in the brain indexes consciousness in noncommunicative patients. Curr Biol 2013; 23: 1914-9
21. Rembado I, Castagnola E, Turella L, Ius T, Budai R, Ansaldo A, Angotzi GN, Debertoldi F, Ricci D, Skrap M, Fadiga L: Independent Component Decomposition of Human Somatosensory Evoked Potentials Recorded by Micro-Electrocorticography. Int J Neural Syst 2017; 27: 1650052
22. Watts AD, Herrick IA, McLachlan RS, Craen RA, Gelb AW: The effect of sevoflurane and isoflurane anesthesia on interictal spike activity among patients with refractory epilepsy. Anesth Analg 1999; 89: 1275-81
23. Chui J, Manninen P, Valiante T, Venkatraghavan L: The anesthetic considerations of intraoperative electrocorticography during epilepsy surgery. Anesth Analg 2013; 117: 479-86
24. Chaitanya G, Arivazhagan A, Sinha S, Reddy KR, Thennarasu K, Bharath RD, Rao MB, Chandramouli BA, Satishchandra P: Dexmedetomidine anesthesia enhances spike generation during intra-operative electrocorticography: A promising adjunct for epilepsy surgery. Epilepsy Res 2015; 109: 65-71
25. Soriano SG, Eldredge EA, Wang FK, Kull L, Madsen JR, Black PM, Riviello JJ, Rockoff MA:

The effect of propofol on intraoperative electrocorticography and cortical stimulation during awake craniotomies in children. Pediatric Anesthesia 2000; 10: 29-34

26. Nenadic Z, Burdick JW: Spike detection using the continuous wavelet transform. IEEE Transactions on Biomedical Engineering 2005; 52: 74-87

27. Lodder SS, van Putten MJ: A self-adapting system for the automated detection of inter-ictal epileptiform discharges. PLoS One 2014; 9: e85180

28. Li X, Cui S, Voss LJ: Using permutation entropy to measure the electroencephalographic effects of sevoflurane. Anesthesiology 2008; 109: 448-56

29. Khadem A, Hossein-Zadeh GA: Quantification of the effects of volume conduction on the EEG/MEG connectivity estimates: an index of sensitivity to brain interactions. Physiol Meas 2014; 35: 2149-64

30. Whitmer D, Worrell G, Stead M, Lee IK, Makeig S: Utility of independent component analysis for interpretation of intracranial EEG. Front Hum Neurosci 2010; 4: 184

31. Zhou D, Thompson WK, Siegle G: MATLAB toolbox for functional connectivity. Neuroimage 2009; 47: 1590-607

32. Hindriks R, Micheli C, Bosman CA, Oostenveld R, Lewis C, Mantini D, Fries P, Deco G: Source-reconstruction of the sensorimotor network from resting-state macaque electrocorticography. Neuroimage 2018; 181: 347-358

33. Schoffelen JM, Gross J: Source connectivity analysis with MEG and EEG. Hum Brain Mapp 2009; 30: 1857-65

34. Cao C, Slobounov S: Alteration of cortical functional connectivity as a result of traumatic brain injury revealed by graph theory, ICA, and sLORETA analyses of EEG signals. IEEE Transactions on Neural Systems and Rehabilitation Engineering 2010; 18: 11-19

35. Stam CJ, Nolte G, Daffertshofer A: Phase lag index: assessment of functional connectivity from multi channel EEG and MEG with diminished bias from common sources. Hum Brain Mapp 2007; 28: 1178-93

36. Vinck M, Oostenveld R, van Wingerden M, Battaglia F, Pennartz CM: An improved index of phase-synchronization for electrophysiological data in the presence of volume-conduction, noise and sample-size bias. Neuroimage 2011; 55: 1548-65

37. Nolte G, Bai O, Wheaton L, Mari Z, Vorbach S, Hallett M: Identifying true brain interaction from EEG data using the imaginary part of coherency. Clinical neurophysiology 2004; 115: 2292-2307

38. Stam CJ, van Straaten EC: Go with the flow: use of a directed phase lag index (dPLI) to characterize patterns of phase relations in a large-scale model of brain dynamics. Neuroimage 2012; 62: 1415-1428

39. Burns SP, Santaniello S, Yaffe RB, Jouny CC, Crone NE, Bergey GK, Anderson WS, Sarma SV: Network dynamics of the brain and influence of the epileptic seizure onset zone. Proc Natl Acad Sci U S A 2014; 111: E5321-30

40. Keller CJ, Honey CJ, Megevand P, Entz L, Ulbert I, Mehta AD: Mapping human brain networks with cortico-cortical evoked potentials. Philos Trans R Soc Lond B Biol Sci 2014; 369

41. Collard MJ, Fifer MS, Benz HL, McMullen DP, Wang Y, Milsap GW, Korzeniewska A, Crone NE: Cortical subnetwork dynamics during human language tasks. Neuroimage 2016; 135: 261-72

42. Fischer F, Pieper F, Galindo-Leon E, Engler G, Hilgetag CC, Engel AK: Intrinsic Functional Connectivity Resembles Cortical Architecture at Various Levels of Isoflurane Anesthesia. Cereb Cortex 2018; 28: 2991-3003

43. Kayser J, Tenke CE: Principal components analysis of Laplacian waveforms as a generic method for identifying ERP generator patterns: I. Evaluation with auditory oddball tasks. Clinical neurophysiology 2006; 117: 348-368

44. Gugino L, Chabot R, Prichep L, John E, Formanek V, Aglio L: Quantitative EEG changes associated with loss and return of consciousness in healthy adult volunteers anaesthetized with propofol or sevoflurane. British Journal of Anaesthesia 2001; 87: 421-428

45. Sanders R, Mostert N, Lindroth H, Tononi G, Sleigh J: Is consciousness frontal? Two perioperative case reports that challenge that concept. British Journal of Anaesthesia 2018; 121: 330-332

46. Lee U, Mashour GA, Kim S, Noh GJ, Choi BM: Propofol induction reduces the capacity for neural information integration: implications for the mechanism of consciousness and general anesthesia. Conscious Cogn 2009; 18: 56-64

47. Lee U, Kim S, Noh GJ, Choi BM, Hwang E, Mashour GA: The directionality and functional organization of frontoparietal connectivity during consciousness and anesthesia in humans. Conscious Cogn 2009; 18: 1069-78

48. Lobo FA, Schraag S: Limitations of anaesthesia depth monitoring. Curr Opin Anaesthesiol 2011; 24: 657-64

49. Blain-Moraes S, Tarnal V, Vanini G, Alexander A, Rosen D, Shortal B, Janke E, Mashour GA: Neurophysiological correlates of sevoflurane-induced unconsciousness. Anesthesiology 2015; 122: 307-16

50. Purdon PL, Pavone KJ, Akeju O, Smith AC, Sampson AL, Lee J, Zhou DW, Solt K, Brown EN: The Ageing Brain: Age-dependent changes in the electroencephalogram during propofol and sevoflurane general anaesthesia. Br J Anaesth 2015; 115 Suppl 1: i46-i57

51. Cornelissen L, Kim SE, Purdon PL, Brown EN, Berde CB: Age-dependent electroencephalogram (EEG) patterns during sevoflurane general anesthesia in infants. Elife 2015; 4: e06513

52. Akeju O, Pavone KJ, Thum JA, Firth PG, Westover MB, Puglia M, Shank ES, Brown EN, Purdon PL: Age-dependency of sevoflurane-induced electroencephalogram dynamics in children. Br J Anaesth 2015; 115 Suppl 1: i66-i76